Elevated Calprotectin and Abnormal Myeloid Cell Subsets Discriminate Severe from Mild COVID-19

Aymeric Silvin, Nicolas Chapuis, Garett Dunsmore, Anne-Gaëlle Goubet, Agathe Dubuisson, Lisa Derosa, Carole Almire, Clémence Hénon, Olivier Kosmider, Nathalie Droin, et al.

▶ **To cite this version:**

Aymeric Silvin, Nicolas Chapuis, Garett Dunsmore, Anne-Gaëlle Goubet, Agathe Dubuisson, et al.. Elevated Calprotectin and Abnormal Myeloid Cell Subsets Discriminate Severe from Mild COVID-19. Cell, 2020, 182, pp.1401 - 1418.e18. ⟨10.1016/j.cell.2020.08.002⟩. ⟨hal-03491454⟩

HAL Id: hal-03491454

https://hal.science/hal-03491454v1

Submitted on 21 Sep 2022

HAL is a multi-disciplinary open access archive for the deposit and dissemination of scientific research documents, whether they are published or not. The documents may come from teaching and research institutions in France or abroad, or from public or private research centers.

L'archive ouverte pluridisciplinaire **HAL**, est destinée au dépôt et à la diffusion de documents scientifiques de niveau recherche, publiés ou non, émanant des établissements d'enseignement et de recherche français ou étrangers, des laboratoires publics ou privés.

Distributed under a Creative Commons CC BY-NC 4.0 - Attribution - Non-commercial use - International License

Version of Record: https://www.sciencedirect.com/science/article/pii/S0092867420309934
Manuscript_1d9bf6c16f7eca4a5b44b7e487987a50

Elevated calprotectin and abnormal myeloid cell subsets discriminate severe from mild COVID-19

Aymeric Silvin,[1] Nicolas Chapuis,[2,3] Garett Dunsmore,[1] Anne-Gaëlle Goubet,[1] Agathe Dubuisson,[1] Lisa Derosa,[1,4] Carole Almire,[3] Clémence Hénon,[5] Olivier Kosmider,[2,3] Nathalie Droin,[6,7] Philippe Rameau,[7] Cyril Catelain,[7] Alexia Alfaro,[7] Charles Dussiau,[2,3] Chloé Friedrich,[2,3] Elise Sourdeau,[8] Nathalie Marin,[9] Tali-Anne Szwebel,[10] Delphine Cantin,[8] Luc Mouthon,[2,10] Didier Borderie,[11] Marc Deloger,[7] Delphine Bredel,[1] Severine Mouraud,[1] Damien Drubay,[12] Muriel Andrieu,[2] Anne-Sophie Lhonneur,[13] Véronique Saada,[14] Annabelle Stoclin,[15] Christophe Willekens,[6,16] Fanny Pommeret[4], Frank Griscelli,[4,14] Lai Guan Ng,[17] Zheng Zhang,[18] Pierre Bost,[19,20] Ido Amit,[20] Fabrice Barlesi,[4] Aurélien Marabelle,[1,21] Frédéric Pène,[2,9] Bertrand Gachot,[15] Fabrice André,[4,5,22] Laurence Zitvogel,[1,22,23] Florent Ginhoux,[17,24,25*,#] Michaela Fontenay,[2,3*] and Eric Solary[6,15,22*]

1. INSERM U1015, Gustave Roussy Cancer Campus, 94800 Villejuif, France.
2. Université de Paris, Institut Cochin, CNRS UMR8104, INSERM U1016, 75006 Paris, France.
3. Service d'hématologie biologique, AP-HP, Hôpital Cochin, 75014 Paris, France.
4. Département d'Oncologie Médicale, Gustave Roussy Cancer Campus, 94800 Villejuif, France.
5. INSERM U981, Gustave Roussy Cancer Campus, 94800 Villejuif, France.
6. INSERM U1287, Gustave Roussy Cancer Campus, 94800 Villejuif, France.
7. INSERM US23, CNRS UMS 3655, Gustave Roussy Cancer Campus, 94800 Villejuif, France.
8. Service des Urgences, AP-HP, Hôpital Hôtel-Dieu, 75014 Paris, France.
9. Service de Médecine Intensive et Réanimation, AP-HP, Hôpital Cochin, 75014 Paris, France.
10. Service de Médecine Interne, AP-HP, Hôpital Cochin, 75014 Paris, France.
11. Service de Diagnostic Biologique Automatisé, AP-HP, Hôpital Cochin, 75014 Paris, France.
12. INSERM U1018, Gustave Roussy Cancer Campus, 94800 Villejuif, France.
13. Laboratoire de virologie, AP-HP, Hôpital Cochin, 75014 Paris, France.
14. Département de biologie et pathologie, Gustave Roussy Cancer Campus, 94800 Villejuif, France.
15. Service de réanimation médicale, Gustave Roussy Cancer Campus, 94800 Villejuif, France.
16. Département d'hématologie, Gustave Roussy Cancer Campus, 94800 Villejuif, France.
17. Singapore Immunology Network (SIgN), Agency for Science, Technology and Research (A*STAR), 8A Biomedical Grove, Immunos Building #3-4, Biopolis, Singapore 138648, Singapore.
18. Institute for Hepatology, National Clinical Research Center for Infectious Disease, Shenzhen Third People's Hospital, School of Medicine, Southern University of Science and Technology, Shenzhen 518112, Guangdong Province, China
19. Systems Biology Group, Department of Computational Biology and USR 3756, Institut Pasteur and CNRS, 75015 Paris, France.
20. Department of Immunology, Weizmann Institute of Science, Rehovot, Israel.

© 2020 published by Elsevier. This manuscript is made available under the CC BY NC user license
https://creativecommons.org/licenses/by-nc/4.0/

21. Département d'Innovation Thérapeutique et d'Essais Précoces (DITEP), Gustave Roussy Cancer Campus, 94800 Villejuif, France.
22. Université Paris-Saclay, Faculté de Médecine, 94270 Le Kremlin-Bicêtre, France.
23. Centre d'investigation clinique - biothérapie, INSERM CICBT1428, 94800 Villejuif, France.
24. Shanghai Institute of Immunology, Shanghai JiaoTong University School of Medicine, 280 South Chongqing Road, Shanghai 200025, China.
25. Translational Immunology Institute, SingHealth Duke-NUS Academic Medical Centre, 169856, Singapore.

* These authors contributed equally.
# Lead contact: Florent Ginhoux, Florent_ginhoux@immunol.a-star.edu.sg

Correspondence to
Florent_Ginhoux@immunol.a-star.edu.sg (F.G.)
Michaela.Fontenay@aphp.fr (M.F)
Eric.Solary@gustaveroussy.fr (E.S.)

Summary

Blood myeloid cells are known to be dysregulated in the coronavirus disease 2019 (COVID-19) caused by SARS-CoV-2. It is unknown whether the innate myeloid response differs with disease severity, and whether markers of innate immunity discriminate high risk patients. Thus, we performed high dimensional flow cytometry and single cell RNA sequencing of COVID-19 patient peripheral blood cells and detected the disappearance of non-classical $CD14^{Low}CD16^{High}$ monocytes, the accumulation of $HLA\text{-}DR^{Low}$ classical monocytes, and the release of massive amounts of calprotectin (S100A8/S100A9) in severe cases. Immature $CD10^{Low}CD101^{-}CXCR4^{+/-}$ neutrophils with an immuno-suppressive profile accumulated as well in blood and lungs, suggesting emergency myelopoiesis. We finally showed that calprotectin plasma level and a routine flow cytometry assay detecting decreased frequencies of non-classical monocytes could discriminate patients who develop a severe COVID-19 form, suggesting a predictive value that deserves prospective evaluation.

Keywords: COVID-19, calprotectin, emergency myelopoiesis, monocyte subsets, neutrophils, S100A8, S100A9, SARS-CoV-2, type I interferon.

Introduction

Coronavirus disease 2019 (COVID-19) is caused by severe acute respiratory syndrome-coronavirus 2 (SARS-CoV-2), which infects the lungs leading to fever, cough and dyspnea (Guan and Zhong, 2020). Most patients presenting with mild disease develop an efficient immune response (Thevarajan et al., 2020), but some go on to develop acute respiratory distress syndrome leading to admission in intensive care unit (ICU), often culminating in multi-organ dysfunction and death (Wang et al., 2020).

In addition to cell autonomous effects of the viral infection, a dysregulated immune response participates in the sudden deterioration of COVID-19 patients, ultimately overwhelming infected and non-infected tissues (Vabret et al., 2020). This overt inflammatory response centers around a cytokine storm (Chen et al., 2020a) with elevated blood concentrations of interleukin-6 (IL-6). Accordingly, therapeutic agents targeting the IL-6/IL-6R-gp130 axis can alleviate the inflammatory response (Michot et al., 2020) and ameliorate immune dysregulation (Giamarellos-Bourboulis et al., 2020), emphasizing the clinical significance of this cytokine. A marked lymphocytopenia is also associated with COVID-19 severity (Chen et al., 2020a); however, the primary source both of the cytokine storm and the mechanisms behind the lymphocytopenia remains elusive (Li et al., 2020).

A growing body of evidence points to dysregulation of innate immune cells of the granulomonocytic lineage during lung viral infections. A variety of human viruses infects monocytes and macrophages to spread through the tissues (Al-Qahtani et al., 2017; Desforges et al., 2007; Nottet et al., 1996; Smith et al., 2004; Yilla et al., 2005). SARS-CoV-2 mRNA is detectable in lung monocytes/macrophages of severe COVID-19 patients (Bost et al., 2020), though its ability to enter these cells in the peripheral blood and activate them directly remains unclear. Also, tissue damage induced by SARS-CoV-2 infection may lead to the release of pathogen- and damage-associated molecular patterns that, in turn induce the activation and recruitment of inflammatory cytokine- and chemokine- producing innate immune cells in an amplifying loop (Liao et al., 2020).

It remains unclear to what extent immune patterns associated with COVID-19 pathophysiology are causative and exacerbating the disease and/or could be used for accurate patient stratification. Here, using high dimensional single cell approaches including single cell RNA sequencing, mass cytometry and 25-parameter spectral flow cytometry, we show that patients doomed to develop a severe disease exhibit a massive release of S100A8/S100A9 calprotectin accompanied by changes in monocyte and neutrophil subsets. We further discover that this pathological immune system reorganization is initiated by the onset of an emergency myelopoiesis that release immature myeloid cells with an immuno-suppressive phenotype into peripheral blood and lungs. Together, our study integrates frequencies of non-classical monocytes and immature neutrophils with calprotectin plasma level as robust biomarkers of COVID-19 severity, suggesting potential therapeutic strategies targeting calprotectin to alleviate severe COVID-19.

Results

Introduction to the patient cohort

This non-interventional study enrolled 158 patients (**Table S1**), including 86 and 72 subjects referred to the hospital with various flu-like symptoms who were diagnosed or not with COVID-19, based on positive and negative RT-PCR on pharyngeal swabs respectively. Patients were stratified according to disease severity: mild disease (n=27) was defined as having no or limited clinical symptoms and not requiring CT-scan or hospitalization; moderate disease (n=16) was defined as being symptomatic, with dyspnea and radiological findings of pneumonia on thoracic CT scan, requiring hospitalization but with a maximum of 9 L/min of oxygen; and severe disease (n=43) was defined as respiratory distress requiring admission into the intensive care unit (ICU). Mild and moderate cases were mixed in the discovery part of the study and considered separately to explore the ability of a routine flow assay to discriminate patients that require hospitalization.

Circulating innate immune cells in mild and severe COVID-19 patients exhibit distinct phenotypes

In order to explore changes induced by SARS-CoV-2 infection in circulating immune cell phenotype, we first collected peripheral blood samples from a discovery cohort of 13 patients positive for SARS-CoV-2 (hereafter "COVID-19 patients") by RT-PCR and 12 patients suffering from flu-like symptoms but negative for SARS-CoV-2. The former group included 5 patients with mild disease and 8 patients with severe COVID-19 (**Table S2)**. After red blood cell lysis, we labelled peripheral blood cells with a panel of 25 antibodies recognizing immune cell surface markers (**Key Resource Table**) and analyzed them by spectral flow cytometry (**Figure 1A, S1A and S1B**). By pooling the data from the 25 control and COVID-19 patients and subjecting them to dimensionality reduction using the non-supervised UMAP algorithm (Becht et al., 2018), we identified populations of $CD4^+$ T cells, $CD8^+$ T cells, $CD19^+$ B cells, $CD14^{High}$ monocytes and $CD15^+CD66b^+$ neutrophils (**Figure 1B and 1C**). We also identified HLA-$DR^{High}CD11b^+$ and $CD16^{High}$ monocytes as well as neutrophils expressing CD11b, CD15, CD16 and CD64 (**Figure 1B and 1C**). Analysis and visualization, using UMAP dimensionality reduction to the cell surface marker expression datasets from control, and mild and severe COVID-19 groups, suggested differences in the repartition of cell populations (**Figure 1D**).

Severe patients exhibited an expansion in the proportion of circulating neutrophils within the peripheral blood cell population (**Figure 1E**), which was associated with an increase in their absolute number (**Table S2**), as already reported (Huang et al., 2020). Focusing on neutrophil subsets, we noticed a slight increase in the fraction of $CD10^{Low}CD101^+$ neutrophils in mild COVID-19 patients (**Figure 1F**), whereas the fraction of $CD10^{Low}CD101^-$ neutrophils was remarkably amplified in severe patients, suggesting an accumulation of immature

subsets of neutrophils (Ng et al., 2019) in the peripheral blood of these patients (**Figure 1G and S1C-E**).

In severe patients, the absolute number of circulating monocytes (**Table S2**) and the proportion of total monocytes among peripheral blood leucocytes (**Figure 1H and S1F**) were similar to controls, but we noticed changes in monocyte subset repartition. The fraction of $CD14^{High}CD16^{High}$ intermediate monocytes was significantly greater in mild COVID-19 patients (16.95+/- 6.75%) than in control (5.84+/-1.02%) or severe (6.77+/-1.10%) groups, while the non-classical $CD14^{Low}CD16^{High}$ monocyte fraction was lower in severe COVID-19 patients (1.31+/-0.35%) than in mild (5.46+/-1.57%) or control groups (6.68+/-1.14%) (**Figure 1I and 1J**). Within the $CD14^{High}CD16^{Low}$ classical monocyte subset (**Figure S1G**), we detected higher frequencies of $CD11b^{High}$ monocytes with increased disease severity (**Figure S1H**), while the intensity of HLA-DR expression was lower across both $CD11b^{+}$ and $CD11b^{-}$ monocyte populations of severe COVID-19 patients (**Figure 1K and 1L**).

Changes in myeloid cell repartition observed in severe patients were associated with lower frequencies of B cells compared to controls ($p<0.001$), and of $CD4^{+}$ ($p<0.001$) and $CD8^{+}$ T cells ($p<0.01$) relative to both controls and mild patients, while $CD56^{+}$ NK cell frequencies remained comparable across all groups (**Figure 1M**).

Altogether, these data suggested SARS-CoV-2-induced changes in the relative abundance of monocyte and neutrophil subsets within the peripheral blood cell population, with loss of non-classical $CD14^{Low}CD16^{High}$ monocytes, reduced expression of HLA-DR on classical monocytes and drop in CD101 and CD10 expression on neutrophils, characterizing severe cases.

Serial single cell analysis of mild versus severe patient blood cells identifies dynamic changes in monocyte subsets

As a second step in our discovery process, we collected peripheral blood samples from three control patients with flu-like symptoms tested negative for SARS-CoV-2, and three SARS2-CoV-2 positive patients, one outpatient with mild disease and two patients with severe disease admitted to ICU (**Figure 2A and 2B**; **Table S3**). Using the 10X Chromium droplet-based platform, these samples were subjected to single cell RNA sequencing (scRNAseq) immediately after collection and red blood cell lysis, without additional sorting or freezing, in an attempt to preserve fragile cell populations, mainly neutrophils. Unsupervised clustering based on gene expression identified B and T cells as well as neutrophils, monocytes, erythroid cells and platelets (**Figure 2C and Figure S2A and S2B**). Samples analyzed by scRNAseq were simultaneously analyzed by spectral flow cytometry for comparison (**Figure 2D**). UMAP analysis of spectral flow cytometry data suggested lower proportions of $CD4^{+}$ and $CD8^{+}$ T cells while the neutrophil fraction was greater in severe patients compared to controls and to the unique mild patient (**Figure 2E and S2C**). The three SARS2-CoV-2-infected

patients were sampled again 10 days later to monitor progression of the immune response in relation to clinical status (**Figure 2A to 2E**).

UMAP visualization of monocytes analyzed by scRNAseq identified three clusters (**Figure 3A**), that may correspond to well-defined monocyte subsets (Guillams et al., 2018). Cells of cluster 1 expressed *CD14*, *ITGAM* (encoding CD11b) and *KLF4* while poorly expressing *FCGR3A* (encoding CD16), suggesting classical monocytes. Cells of cluster 3, which expressed high levels of *FCGR3A* and low levels of *CD14,* may correspond to non-classical monocytes, and cluster 2, in which cells expressed both *CD14* and *FCGR3A*, evoked intermediate monocytes (**Figure 3A**). Differential expressed genes (DEGs) and pathway analyses delineated a type I interferon signature in the mild COVID-19 patient monocytes (**Figure 3B, S3A and S3B; Table S4**). This signature was less pronounced in the two severe COVID-19 samples, contrasting with the elevated expression of genes involved in the production of reactive oxygen species (ROS) and nitric oxygen species (NOS) (**Figure S3A and S3B**).

A non-supervised UMAP analysis of the data collected by spectral flow cytometry of the same samples detected variations in monocyte subset repartition among patients: compared to controls and the mild patient, severe patient #1 showed a lower fraction of $CD14^{Low}CD16^{High}$ non-classical monocytes at day 0 while the other severe patient showed a high level of this monocyte fraction (**Figure 3C**). Additionally, the two severe patients showed markedly higher levels of classical $CD14^{High}CD16^{Low}$ monocytes, expressing more CD141 (*THBD*) at their surface (**Figure 3D**), in accordance with the scRNAseq analysis (**Table S4**).

In the mild patient, one of the most highly expressed genes in classical monocytes was the interferon stimulated gene (Sevelsted et al., 2015) *SIGLEC-1*, consistent with the high level of expression of CD169, the corresponding protein, at the surface of classical monocytes at day 0 (**Figure 3E**). Ten days later, *SIGLEC-1* gene expression was down-regulated and CD169 expression was undetectable at the surface of HLA-DR^{High} classical monocytes (**Figure 3B and 3E)**. The two severe patients exhibited low expression of HLA-DR protein on their monocyte surface at day 0, without significant change at day 10 (**Figure 3E)**.

Validating these discovery experiments, we performed mass cytometry analysis of an independent cohort of 12 patients (four in each group; control, mild and severe) (**Table S5**), which showed a lower fraction of $CD14^{Low}CD16^{High}$ non-classical monocytes in severe compared to mild patients (**Figure 3F and 3G**). In accordance with pathway analysis of scRNAseq data highlighting NF-κB activation as a prominent feature in monocytes of severe patients (**Figure 3B and S3B**), we observed significantly higher levels of the phosphorylated transcription factor RelA/p65 (P-p65), a critical effector of the canonical NF-κB pathway, in HLA-$DR^{Low}CD14^{High}$ classical monocytes from severe patients compared to controls (**Figure 3H and 3I**). We also measured P-p65 expression in circulating $CD34^{+}$ cells, identifying increased expression in severe disease (**Figure S3C**).

Serial single cell analysis of mild versus severe patient blood cells identifies changes in neutrophil subsets

UMAP analysis of neutrophils identified two clusters (**Figure 4A**). We observed an increase of cluster 2 cells in severe COVID-19 patients (**Figure 4B**). Cluster 1 expressed *IL1R2* gene whereas cluster 2 expressed also high levels of *S100A8* and *S100A9, CXCR4, SELL* and *SPI1* (**Figure 4C and S4A**). DEGs and pathway analyses in mild patient neutrophils informed of a type I interferon response at day 0 that was lost by day 10 (**Figure 4D, S4B and S4C**). This signature was absent in controls and also in the two severe patient samples collected at later time-points (**Figure 4D**), demonstrating high expression of genes involved in the production of ROS, the inducible NOS pathway, IL-1 signaling and NF-κB activation pathways (**Figure S4B and S4C**).

Analysis of the data collected by spectral flow cytometry of the same samples distinguished $CD10^{+}CD101^{+}$ mature neutrophils from $CD10^{Low}CD101^{-}$ immature neutrophils. At day 0, the two severe patients had more circulating $CD10^{Low}CD101^{-}$ immature neutrophils compared to controls or the mild patient (**Figure 4E**). Severe patient #1 neutrophils had increased the expression of CD101 on their surface at day 10 while severe patient #2 neutrophils retained their immature phenotype at day 10. Focusing on the expression of a pre-neutrophil hallmark CXCR4 at the surface of $CD10^{Low}CD101^{-}$ immature neutrophils (Ng et al., 2019), we observed an increase in the proportion of neutrophils with a $CD10^{Low}CD101^{-}CXCR4^{+}$ phenotype, which presumably are pre-neutrophils (**Figure 4F**). Mass cytometry analysis of an independent cohort of 12 patients (four controls, four mild and four severe COVID patients, **Table S5**) again suggested a higher fraction of $CD10^{Low}CD101^{-}$ immature neutrophils in severe patients compared to control patients (**Figure 4G and 4H**).

Altogether, results of these exploratory scRNAseq experiments identified a transient type I interferon response in cells of a patient with a mild disease and the presence of phenotypically immature subsets of monocytes and neutrophils in two patients with a severe disease, which were further identified by mass cytometry.

Calprotectin plasma levels distinguish mild from severe COVID-19 patients

S100A8 and S100A9 alarmins, representing ~45% of the cytoplasmic proteins in neutrophils, are released under inflammatory conditions and form a stable heterodimer known as "calprotectin" (Wang S et al., 2018). In accordance with preliminary results generated by scRNAseq (**Figure S4A**), RT-qPCR analysis detected higher expression of *S100A8* and *S100A9* genes in peripheral blood nucleated cells of patients with severe COVID-19 (n=8) compared to controls (n=8) and patients with a mild disease (n=16) (**Figure S5A and Table S5**). This led us to measure the plasma level of calprotectin, together with type I interferon (IFNα) and 40 other cytokines and chemokines in samples from a cohort of 84 patients (**Table S6**). As observed in **Figure 5A**, patients with mild disease showed significantly less CXCL8 (**Figure 5C and S5B**) and significantly more type I IFNα (**Figure 5A and 5C**) compared to controls. Severe

patients exhibited dramatically higher calprotectin levels compared to mild COVID-19 or controls, without further increase in IFNα plasma level above mild disease levels (**Figure 5B, 5C and S5C**). Calprotectin was the most significantly increased circulating biomarker in severe patients, accompanied by a rise in 23 other tested chemokines and cytokines, including CXCL-8, CXCL-12 and IL-6 (**Figure 5B, 5C and S5B**).

Age and comorbidities (including obesity, diabetes mellitus, cardiovascular and respiratory diseases and cancer) are predictors of severe COVID-19 disease (Richardson et al., 2020). We found that plasma calprotectin levels were significantly higher in control patients with comorbidities, as well as in mild or severe COVID-19 patients with comorbidities (**Figure 5D**). Nevertheless, the increase in calprotectin in severe COVID-19 far exceeds that correlations associated with comorbidities. None of the other measured circulating proteins were significantly higher in patients with comorbidities (**Figure 5E**). Bacterial infections can occur in severe COVID-19 (Chen et al., 2020c; Llitjos et al., 2020) and were present in some of our severe patients but did not significantly modify the profile of released proteins (**Figure S5B and S5C**), including calprotectin (**Figure 5F**). No correlation between calprotectin and age was observed in each group of patients (**Figure S5D**). Calprotectin concentration correlated with neutrophil counts (**Figure 5G**), fibrinogen plasma levels (**Figure 5H**) and D dimers (**Figure 5I**), the latter being fibrin degradation products reflecting a hypercoagulability state. Modeling calprotectin plasma level using multivariable linear regression to take into account potential confounding factors (age, sex, comorbidities) and the correlation with neutrophil count, fibrinogen et D-dimers, these associations were still statistically significant (neutrophils p-value=1.154e-04; fibrinogen p-value=5.688e-05; D-dimers p-value=2.099e-03). We also uncovered a weak correlation between IL-6 plasma concentration and levels of calprotectin (**Figure S5E**), blood neutrophil count (**Figure 5J**), fibrinogen (**Figure 5K**) and D dimers (**Figure 5L**), which disappeared after adjusted multilinear regression. Finally, a logistic regression including age, sex and comorbidities together with biological parameters identified plasma levels of calprotectin, CX3CL1, CXCL11 and CXCL13 as the parameters that best discriminate controls / mild COVID-19 patients from severe patients.

These results indicate that high plasma levels of calprotectin are seen in severe COVID-19 patient, not in those with a mild disease. Importantly, this increase is independent from confounding factors for prognosis such as advanced age, co-morbidities or concurrent bacterial infection which have only minor effects on plasma calprotectin levels.

Spectral flow analyses validate a contrasted innate immune cell signature in mild versus severe COVID-19

Hypothesis from the scRNAseq-based identification of CD37, CD63 (LAMP3), CD169 (SIGLEC-1) and CD184 (CXCR4) biomarkers of blood cell subsets whose relative proportions differ in mild and severe COVID-19 patients, prompted us to add additional antibodies targeting these proteins to the spectral flow cytometry panel. We applied this new panel to samples

from an independent validation cohort of 90 patients. This cohort included 48 control patients and 42 COVID-19 positive, of which 16 had mild disease and 26 had severe disease (**Figure 6A and Table S6**). Non-supervised analysis and UMAP visualization identified the main cell populations in the three categories of patients combined (**Figure S6A and S6B**). Analyzing patients individually confirmed the significant decrease in B cell, $CD4^+$ T cell and $CD8^+$ T cell fractions in severe patients compared to control and mild groups (**Figure 6B**), which may be a consequence of the increased neutrophil fraction (**Figure 6C**) and absolute number (**Table S6**). Within neutrophils, we observed more specifically a shift in $CD10^{Low}CD101^-$ neutrophils (**Figure 6D and 6E**) and the subset of $CD10^{Low}CD101^-$ neutrophils that express CXCR4 ($CD10^{Low}CD101^-CXCR4^+$ cells) (**Figure 6F**) that we previously observed in severe patients. Finally, the fraction of $CD10^{Low}CD16^{Low}$ neutrophils was also higher in severe patients (**Figure S6C**), further suggesting for the accumulation of immature neutrophils in the blood of severe COVID patients.

ScRNA-seq analyses of monocyte subsets had indicated differential changes in the distribution of non-classical $CD14^{Low}CD16^{High}$ monocyte fractions between the two patients with severe disease (see **Figure 3C**). Since samples were collected from patients at various time points after admission in ICU, we asked if the duration of ICU stay affects the monocyte subset distribution. In the 26 severe patients of this cohort (**Table S6**), we observed a significant correlation between the time spent in ICU and the fraction of non-classical monocyte subset, irrespective of the presence or absence of concurrent bacterial infection (**Figure 6G**). Mean time spent in ICU was 5.46 days for patients with less than 5% non-classical monocytes compared to 8.83 days for those with 5% and more non-classical monocytes (**Figure 6H and 6I**).

Then, we examined other monocyte subsets: in the majority of mild patients, we observed a fraction of classical monocytes that express CD169, which was decreasing in severe patients (**Figure 6J, 6K and S6D**). CD169 expression correlated with plasma levels of IFNα (**Figure S6E**). Independent of the time they spent in ICU, severe patients also showed a larger fraction of classical monocytes expressing high levels of CD141 compared to controls (**Figure 6J and 6L**) and of monocytes expressing low levels of HLA-DR compared to controls and mild patients (**Figure S6F**). Finally, the time spent in ICU did not significantly affect the repartition of lymphocyte populations or neutrophil subsets (**Figure S6F and S6G**).

Thus, severe COVID-19 patients exhibited a transient decrease in non-classical monocyte frequencies, a stable decrease in HLA-$DR^{Low}CD141^+$ classical monocytes and a major increase in $CD10^{Low}CD101^-CXCR4^{+/-}$ immature neutrophils.

High calprotectin level and loss of non-classical monocytes correlate with COVID-19 severity

We next investigated whether changes in circulating myeloid cell phenotypes could be used to discriminate patients who develop severe COVID-19. Within our previous cohort, we

separated mild (n=12) from moderate (n=6) and severe (n=27) patients using clinical criteria. Patients classified as “moderate” demonstrated intermediate changes between those of mild outpatients and severe patients in ICU (**Figure S7A**). The fraction of $CD10^{Low}CD101^{-}$ neutrophils in moderate patients was intermediate but not significantly different to any group (**Figure 7A**). However, the amount of calprotectin measured in moderate COVID-19 patients was significantly higher than mild outpatients but still significantly lower than severe COVID-19 patients (**Figure 7B**). In comparison, IFNα levels were not significantly different between moderate and mild or severe patients (**Figure S7B**). The difference in non-classical monocyte fraction was significant between mild and moderate patients, dropping down to levels comparable to severe cases (**Figure 7C**).

Thus, we hypothesized that the decreased non-classical monocyte fraction could be used as a fast and simple diagnostic test to distinguish moderate from mild COVID-19 cases, especially in cases were clinical symptoms may be substantially overlapping. This would facilitate rapid and accurate identification of currently classified as “mild” patients at the cusp of potentially progressing to more severe disease. We therefore employed a low dimensional flow cytometry approach that measures the fraction of classical ($CD14^{High}CD16^{Low}$), intermediate ($CD14^{High}CD16^{High}$) and non-classical ($CD14^{Low}CD16^{High}$) monocyte subsets among total peripheral blood monocytes, and applied it initially to a learning cohort of 98 patients, consisting of 16 mild, 10 moderate and 16 severe COVID-19 patients, along with 56 controls (**Table S7**). All hospitalized patients were sampled within ten days of admission to limit the potential impact of time in ICU (see **Figure 6G**); the mean time spent in ICU was 5.5 days at the point of sampling. The cohort also included 56 controls. Patients with mild disease showed a fraction of non-classical monocytes similar to that observed in controls. In contrast, moderate patients showed lower levels of non-classical monocytes, as observed in severe patients (**Figure 7D)**. To measure the global performance of this test, we used a receiver operating characteristic (ROC) curve (Hajian-Tilaki, 2013). The point of the ROC corresponding to the best sensitivity/specificity compromise indicated that a non-classical monocyte fraction below 4% separated patients with moderate or severe COVID-19 from those with mild or no disease with 76.9% sensitivity (95% bootstrap confidence interval (BCI) [61.5%; 92.3%]) and 89% specificity (95% BCI [80.6%; 95.8%]) (**Figure S7C**).

We then applied these analyses to blood samples from an independent validation cohort of 24 hospitalized patients from a different clinical center (10 controls, 3 mild, 4 moderate and 7 severe COVID-19 patients) (**Table S7**). A non-classical monocyte fraction below 4% of total circulating monocytes, as defined in the learning cohort, also segregated those with a mild disease from moderate and severe disease with high sensitivity (81.8%, 95% BCI [72.7%; 100%]) and specificity (92.3%, 95% BCI [83.3%; 100%]) (**Figure 7E**). These results confirmed the specificity and sensitivity of our assay to discriminate patients with different COVID-19 severity.

Further confirming these observations, serial sampling of two severe patients who responded to anti-IL-6R antibodies documented that their clinical recovery was associated with the reappearance of non-classical monocytes in the blood (**Figure S7D**). Alongside, one patient who was referred initially with limited symptoms (atypical thoracic pain) and was SARS-Cov-2 PCR negative unexpectedly exhibited a low fraction of non-classical monocytes (3.4%), accompanied by 10% HLA-DR^{Low} classical monocytes. The following day, pulmonary symptoms appeared, the patient was hospitalized requiring oxygen therapy, and a lung CT-scan revealed characteristic COVID-associated injury. Such cases suggest that the loss of non-classical monocyte fraction could be a strong indicator of existing or impending severe COVID-19.

Additional informative parameters could be added to this flow assay to increase its specificity to identify a transition to severe COVID-19, including a decreased expression of HLA-DR at the surface of classical monocytes (**Figure S7E**) that is associated with a decrease in non-classical monocyte fraction below 4% (**Figure S7F**), and an increase in the fraction of CD16^{Low} neutrophils (**Figure S7G**). Comparison of ROC curves indicated that calprotectin plasma level and monocyte or neutrophil subset analyses distinguished mild COVID-19 in outpatients from moderate or severe disease in hospitalized patients, while IFNα2a plasma level did not (**Figure S7H**).

Together with calprotectin plasma level, flow identification of a decrease in non-classical monocyte fraction below 4% of total monocytes could provide improved resolution to clinical observations when categorizing patients at the borders of mild and moderate/severe COVID-19. This would potentially identify those individuals at greatest risk of rapid decline and highlight the need for pro-active management/intervention and intensive monitoring. This assay could be reinforced by analysis of HLA-DR^{Low} classical monocyte and CD16^{Low} neutrophil fractions.

Integration of lung and blood scRNAseq reveals abnormal myeloid cell populations discriminating severe from mild COVID-19

The lungs are a major organ affected in severe COVID-19 patients. To better understand how the distinctive cell signatures found in the blood of severe COVID-19 patients, particularly the presence of immature neutrophils and HLA-DR^{Low} monocytes, affected immune cell compartments in the lungs, we integrated our dataset using the SEURAT V3 pipeline (Stuart et al., 2019) with the published scRNAseq dataset of cells from 12 bronchoalveolar lavage fluids (BALF) of control (n=3), mild (n=3) and severe (n=6) COVID-19 patients (Liao et al., 2020; GSE145926). This analysis provided an unbiased global map of immune cells in the blood and BALF of control, mild and severe COVID-19 patients. Using dimensional reduction, we identified 5 regions based on DEGs across pooled data from all samples (**Figure 7F and S7I**), including T cells (characterized by the expression of genes including *NKG7*, *CD8A*, *CST7*, *GZMB* and *GZMA*), B cells (*IGLV3-19*, *IGHV4-34*, *IGHG1*, *IGHA1* and *JCHAIN*), neutrophils

(*G0S2*, *RSAD2*, *IL1R2* and *IL1RN*), alveolar macrophages (*APOE*, *MSR1*, *MARCO* and *FBP1)* and monocytes/macrophages (*FN1*, *CXCL10*, *CD68* and *NUPR1*). Validating this approach, the alveolar macrophage region was mainly present in BALF of control patients but was dramatically decreased in mild and severe COVID-19 patients and only one cell from our blood scRNAseq matched in this region (**Figure 7F and 7G**). We also observed changes in the monocyte/macrophage region of the BALF from mild or severe patients versus controls and a dramatic neutrophil accumulation in severe disease (**Figure 7G**).

Monocytes/macrophages were increased in BALF of mild compared to control and severe groups (**Figure 7H and 7I**) and these cells were characterized by the expression of the ISGs (*SIGLEC-1*, *IFI44* and *IFITM3*) (**Figure 7J***)* with pathway analyses indicating the upregulation of viral replication and interferon type I signaling pathways. In contrast, NOS biosynthetic process and monocyte chemotaxis were upregulated in BALF monocytes/macrophages of severe patients (**Figure S7J**) that, similar to blood monocytes, expressed lower levels of *HLA-DRA* and *HLA-DRB1* and higher levels of *NFKBIA* mRNA compared to controls or mild COVID-19 patients (**Figure 7J**). Finally, neutrophils were present at high frequencies in BALF from severe COVID-19 patients but not in BALF from controls or mild patients (**Figure 7K and 7L**). UMAP integration of severe patient samples indicated that BALF neutrophils, similar to blood neutrophils (**Figure 7L**), were characterized by high expression of *S100A8, S100A9* as well as *CXCR4*, indicating an immature state, (**Figure 7M, 7N and S7K**).

Altogether, integration of blood and BALF myeloid cells identified in severe COVID-19 patients the loss of *HLA-DRA* and *HLA-DRB1* and high *NFKBIA* expression in monocytes/macrophages (not including alveolar macrophages), together with an accumulation of neutrophils expressing high levels of *S100A8/A9* and *CXCR4*.

Discussion

This study presents evidence that patients who develop a severe COVID-19 exhibit high levels of calprotectin and inflammatory cytokines and chemokines correlating with an emergency myelopoiesis generating ROS- and NOS- expressing immunosuppressive myeloid cells (HLA-DR^{Low} monocytes and immature subsets of neutrophils).

The first line of defense in viral-infected patients typically involves a protective innate response incorporating the transient and strong production of type I IFNs. Through inducing expression of ISGs, type I IFNs inhibits virus replication and promotes an effective innate and adaptive immune response (Thevarajan et al., 2020; Totura and Baric, 2012). This antiviral response may be overflowed in COVID-19 patients who suddenly evolve into clinically threatening disease (Hadjadj et al., 2020). Severe COVID-19 frequently develops in the context of advanced age and comorbidities that provide a degree of underlying systemic chronic inflammation (Furman et al., 2019). Such inflammation could disrupt the timing of type I IFN response relative to the kinetics of virus replication (Teran-Cabanillas and Hernandez, 2017), which was shown to be critical in mouse models of coronavirus infection (Channappanavar et al., 2019). An imbalance between the type I IFN and inflammatory responses could also be favored by the highly efficient replication of SARS-CoV-2 in human tissues (Chu et al., 2020), and by the IFN-neutralizing effects of structural and non-structural viral components shared between SARS-CoV-2 and other virulent human coronaviruses (Chen et al., 2014; Yang et al., 2015).

Severe COVID-19 patients exhibit abnormal partition of circulating monocytes and of neutrophils expressing *S100A8* (*calgranulin A / myeloid-related protein 8*) and *S100A9* (*calgranulin B / myeloid-related protein 14*) alarmin genes. Importantly, an accumulation of neutrophils expressing high levels of *S100A8/A9* genes was also observed in the BALF of these patients. The release of massive amounts of calprotectin, the heterodimer formed by S100A8 and S100A9 proteins, is a striking event associated with severe COVID-19. This heterodimer promotes cell migration and boosts NADPH (Nicotinamide Adenine Dinucleotide Phosphate) oxidase activity. Calprotectin is a TLR4 and RAGE (receptor for advanced glycation end products) ligand that, upstream of TNFα (Vogl et al., 2018) and CXCL8 (Simard et al., 2014) synthesis and secretion, promotes NF-κB activation (Riva et al., 2012) and the secretion of multiple inflammatory proteins as IL-6 (Wang et al., 2018). Thus, we propose that calprotectin may account for, and possibly trigger the cytokine release syndrome that characterizes severe COVID-19. Its production may be amplified by tissue damage, generating a harmful hyper-inflammation loop (Kuipers et al., 2013) that precludes these peptides from exerting more protective functions (Austermann et al., 2014; Freise et al., 2019; Ulas et al., 2017; Vogl et al., 2018). Chronic inflammation from comorbidities may synergize with SARS-CoV-2 viral infection to induce a systemic release of calprotectin, which translate by the up-regulation of NF-KB and the loss of HLA-DR on classical monocytes and the presence of immature neutrophils, altogether converging to a state of chronic inflammatory induced immunosuppression. Abnormal neutrophils were observed previously

in severe COVID-19 patients (Wilk et al., 2020). However, authors concluded that these neutrophils transdifferentiate from B cells. We have no supporting results suggesting that it could be the case.

In healthy conditions, roughly 85% of total circulating monocytes are $CD14^{High}CD16^{Low}$HLA-DR^{High} cells that are rapidly recruited to inflamed tissues (Guilliams et al., 2018). As in other severe illnesses (Lukaszewicz et al., 2009), the expression of HLA-DR on $CD14^{High}$ circulating monocytes is low in severe COVID-19, which correlates with, and could be mediated by, IL-6 overproduction (Giamarellos-Bourboulis et al., 2020). A more specific feature of COVID-19 is the low fraction of $CD14^{Low}CD16^{High}$ non-classical monocytes. This fraction commonly increases in patients with sepsis and inflammatory diseases, including viral infections (Kratofil et al., 2017). The decrease in non-classical monocyte fraction could involve the ability of calprotectin to fasten the trans-endothelial migration of leucocytes (Fassl et al., 2015), unless these cells strongly adhere to the endothelium, or the conversion of classical into non-classical monocytes is stuck (Hanna et al., 2011; Hofer et al., 2015) (Selimoglu-Buet et al., 2018). Whatever the mechanism, the lower than normal frequencies of non-classical monocytes (Thevarajan et al., 2020; Hadjadj J et al., 2020) suggest a SARS-CoV-2 characteristic effect that is not observed in other viral infections. Most importantly, this decrease generates a highly characteristic biological signature of COVID-19's aggressive form, with the potential to be easily measured using standard diagnostic flow cytometry and to provide information on the real-time immunological severity of the infection.

The burst of calprotectin detected in COVID-19 patients may trigger NF-κB-driven emergency myelopoiesis, generating immature and dysplastic cells (Basiorka et al., 2016; Chen et al., 2013). Given the considerable hematopoietic potential of the lung (Lefrancais et al., 2017), the burst of calprotectin could also promote the contribution of lung megakaryocytes to disease pathogenesis in this organ. Whatever the mechanism, the immature and mature cells released into the peripheral blood by emergency myelopoiesis may be endowed with immunosuppressive functions, suggesting that myeloid derived suppressive cells (MDSCs) as detected in cancer, inflammation and other diseases (Veglia et al., 2018) might be important in COVID-19. In addition to HLA-DR^{Low} monocytes whose phenotype is that of monocytic MDSCs (M-MDSCs), $CD10^{Low}CD101^{-}CXCR1^{+}$ immature cells are reminiscent of granulocytic MDSCs (G-MDSCs) (Aarts et al., 2019; Mastio et al., 2019; Veglia et al., 2018). Thus, neutrophil precursors such as the pre-neutrophil (preNeu) population that are CXCR4 positive (Evrard et al., 2018), may be released into the blood from the bone marrow prematurely and infiltrate the lung tissue in severe patients. The emergence of these populations could be a predictor of switch to a severe disease. Further research will be required to determine their specific role in disease development.

Altogether, we observed that severe COVID-19 is specifically associated with 1) a burst of circulating calprotectin that precedes cytokine release syndrome, 2) low levels of non-classical monocytes in the peripheral blood, and 3) an emergency myelopoiesis that releases immature and dysplastic myeloid cells with an immune suppressive phenotype. Calprotectin

plasma level and non-classical monocytes monitoring in the blood of patients could be implemented in a routine lab to discriminate patients with early immunological signs consistent with developing more severe disease, as recently suggested (Chen et al., 2020b). Finally, in addition to the network of potential drug targets recently depicted by analysis of SARS-CoV-2 interactions (Gordon et al., 2020), our work provides further rationale for the testing of several clinical strategies, including: blocking emergency myelopoiesis with Lenzilumab (NCT04351152), a recombinant anti-human GM-CSF antibody (Patnaik et al., 2020); testing the oral quinoline-3-carboxamide Tasquinimod (Fizazi et al., 2017) and related molecules such as ABR-215757 (Paquinimod) which blocks the binding of S100A9 to TLR4 and RAGE (Kraakman et al., 2017; Raquil et al., 2008) and the preclinical anti-CD33 monoclonal antibodies (Walter, 2018) which may prevent the interaction of S100A9 with myeloid progenitors (Eksioglu et al., 2017).

Limitations of the present study

These analysis provide snapshots of the differences in innate immune cell phenotype and calprotectin plasma level between outpatients with a mild disease at the time of sampling, having no or limited clinical symptoms and not requiring CT-scan or hospitalization, and moderate to severe patients whose clinical situation requires hospitalization and, in most cases, oxygen supply. Although all the statistical analyses indicate that these biomarkers efficiently discriminate these two clinical situations and may help for urgent patient triage, a prospective serial analysis is now required to evaluate how these biomarkers can predict the switch from a mild to a moderate or severe COVID-19 and inform on the mechanisms involved in this switch.

Acknowledgements: Our teams are supported by grants from Ligue Nationale Contre le Cancer (Equipes labellisées), Agence Nationale de la Recherche (IHU PRISM), Institut National du Cancer (SIRIC CARPEM and SOCRATE), Fondation ARC, Fondation pour la Recherche Médicale and private donations (Dassault systems, Agnes B, Izipizi, Ralph Lauren, and Malakoff Humanis). Florent Ginhoux is supported by Singapore Immunology Network (SIgN) core funding, a European Molecular Biology Organization (EMBO) YIP awardee and is supported by the Singapore National Research Foundation Senior Investigatorship (NRFI) NRF2016NRF-NRFI001-02. Lai Guan Ng is supported by Singapore Immunology Network (SIgN) core funding. The authors thank Emmanuelle Gallois, Jean-François Méritet and Flore Rosenberg, for SARS-CoV-2 PCR tests, Jean-Daniel Chiche and Jean-Paul Mira (from Medical Intensive Care Unit, Cochin Hospital), Maela Francillette, Betty Leite, Valérie Camara-Clayette (from AMMICa platforms, CRB, Gustave Roussy), Audrey Naimo (from AMMICa platforms, Gustave Roussy), Karine Bailly (from CYBIO platform, Institut Cochin), Jérôme Duchemin, Catherine Gicquel, Amandine Houvert, Georges Jourdi, Françoise Levavasseur, Laurence Marnet, Bruno Montout, Loetitia Rhino, Isabelle Souville, and Christine Scamps, for their technical support, Julien Hadoux and Jean-Marie Michot for providing samples, Dorothée Selimoglu-Buet and Xavier Mariette for helpful scientific discussions. We thank Dr Lucy Robinson (Insight Editing London) for editing of the manuscript.

Author Contributions: Conceptualization, A.Si, N.C., F.Gi, M.F., and E.Sol; Methodology, L.G.N., I.A., Z.Z., I.A., L.Z., and B.G.; Investigation, G.D., A-G.G., A.D., C.A., C.H., O.K., N.D., P.R., C.C., C.D., C.F., D.C., D.B., S.M., M.A., A-S.L., V.S., F.Gr., and P.B.; Formal analysis, N.C., G.D., A.A., M.D., and D.D.; Funding acquisition, A.M., F.A., L.Z., F.Gi., M.F., and E.Sol.; Resources, L.D., E.Sou, N.M., T-A.S, D.C., L.M., A.St., C.W., F.Po., F.B., A.M., and F.Pe.; Data curation, L.D., C.A., C.H., and M.F.; Validation, M.F., and E.Sol.; Visualization, A.Si., G.D., A-G.G, A.D., F.Gi., M.F., and E.Sol.; Writing – Original Draft, E.Sol.; Writing, review, editing, A.Si., F.Gi., M.F., and E.Sol.; Supervision: F.Gi., M.F., and E.Sol.

Declaration of Interests: The authors do not have any conflict of interest to declare. Aymeric Silvin, Nicolas Chapuis, Michaela Fontenay, Eric Solary and Florent Ginhoux are the inventors of a patent EP 20305624.7 “Methods for detecting and treating COVID patients requiring intensive care” submitted June 9th 2020 under Gustave Roussy name.

Main figure titles and legends

Figure 1. Spectral flow analysis of peripheral blood cells in a learning cohort of controls and COVID-19 patients. A. Peripheral blood samples collection pipeline; **B.** Non-supervised UMAP analysis of data from 25 patients (controls=12; mild=5; critical=8); **C.** Cell surface marker expression within UMAP analysis shown in panel B; **D.** Non-supervised UMAP analysis of patient blood samples in control, mild and severe groups; **E.** Percentage of neutrophils within total cells in each individual sample within indicated patient groups; **F.** Partition of neutrophil subsets, based on CD101 and CD10 expression, within each patient group (data pooled per group); **G.** Percentage of $CD10^{Low}CD101^{+/-}$ neutrophils among total neutrophils, as in E; **H.** Percentage of monocytes within total cells, as in E . **I.** Partition of monocyte subsets in in each individual sample within patient groups, based on CD14 and CD16 expression (left panels) or CD11b and HLA-DR expression (right panels); **J.** Fractions of non-classical monocytes within total monocytes, as in E ; **K.** CD11b and HLA-DR expression on classical monocytes within each patient group (data pooled per group); **L.** Percentage of $HLA\text{-}DR^{low}$ classical monocytes within classical monocytes, as in E; **M.** Percentage of B, $CD4^+$ T, $CD8^+$ T, and NK cells within total cells, as in E; Kruskal-Wallis test, * $P<0.05$; ** $P<0.01$; *** $P<0.001$; ns, non-significant.

Figure 2. Single cell RNA sequencing of peripheral blood cells in SARS-CoV-negative and positive patients. A. Two blood samples were collected ten days apart from 3 COVID-19 patients. Blood was also collected once from 3 outpatient controls whose SARS-CoV-2 RT-PCR was negative. Individual cell mRNAs were sequenced using Chromium 10X technology; **B.** Time line of sample collection in the three patients; further details in **Table S4**; **C.** UMAP analysis of the 9 sequenced samples showing the repartition of indicated cell populations. Patient samples were analyzed individually at days 0 and 10; control patients (individual analyses, f**igure S2**); **D.** Spectral flow cytometry analysis of surface marker expression performed on the same samples; **E.** UMAP analysis of cell populations detected by spectral flow cytometry data in each patient at day 0 and at day 10 and controls (individual analyses, **figure S2**).

Figure 3. Single cell analysis of monocytes by single cell RNA sequencing, spectral flow cytometry and mass cytometry. A. UMAP profile of monocytes in samples described in **Figure 2A**, and violin plots of gene expression in three statistically defined clusters; **B.** Heatmap of differentially expressed genes (DEGs; logFC ± 0.25; FDR<0.05) in total monocytes; columns labelled "0" identifies DEGs generated by comparing each patient sample at day 0 to the pool of the three controls and the two other patient samples at day 0; columns labelled "10" identifies the expression of these genes in each patient sample at day 10 compared to day 0; genes shown in **Table S4**. **C-E**. Spectral flow analysis in pooled controls and each individual patient sample at day 0 and day 10 of monocyte subset partition in samples analyzed by scRNAseq (**C**), CD11b and CD141 expression among classical

monocytes (**D**), and CD169 and HLA-DR expression among classical monocytes (**E**); **F-I.** Mass cytometry analysis of monocyte subsets in 4 patients within each group (pooled data) (**F)**; non-classical monocyte fraction among total monocytes in each individual sample within the 3 groups (**G**); p65/NF-κB expression in HLA-DR^{low} classical monocyte subset as in F (**H)**; fraction of p65/NF-κB^{high}HLA-DR^{low} classical monocytes among classical monocytes as in G (**I)**.

Figure 4. Single cell analysis of neutrophils by single cell RNA sequencing, spectral flow cytometry and mass cytometry. A. UMAP profile of neutrophils in the 9 samples analyzed as described in **Figure 2A**; **B.** UMAP profile of neutrophils within the 3 controls, the mild and the two severe cases with the cluster gates overlaid; **C.** Violin plots of indicated gene expression in two statistically defined neutrophil clusters; **D.** Heatmap of DEGs in total neutrophils generated as described in Figure 3B; **E-F.** Spectral flow analysis in pooled controls and each individual patient sample at day 0 and day 10 of neutrophil subsets, based on CD10 and CD101 expression (**E**), and CXCR4 and CD11b expression among CD10^{Low}CD101^{-} neutrophils (**F**) in indicated samples (pooled controls). **G-H.** Mass cytometry analysis of neutrophil subsets in 4 patients within each group (pooled data) as in Figure 3F-I, based on CD10 and CD101 expression (**G**) and the fraction of CD10^{Low}CD101^{-} neutrophils among total neutrophils in each sample within the 3 groups (**H**).

Figure 5. Calprotectin is the most abundant immune mediator detected in the plasma of severe COVID-19 patients. Plasma levels of calprotectin (S100A8/S100A9), Interferon alpha (IFNα2a) and 40 cytokines and chemokines in blood samples collected from 84 patients (controls, 40; mild disease, 18; moderate or severe disease, 25). **A.** Volcanoplot representation of cytokine levels in mild COVID-19 compared to controls; IFNα2a shown in orange, **B.** Volcanoplot representation of cytokine levels in severe COVID-19 compared to control patients; IFNα2a shown in orange, calprotectin, CXCL11, CXCL13 and CX3CL1 in red being are the most significantly associated with severe forms; **C.** Circulating levels of CXCL8, IFNα2a, calprotectin and IL-6 in individual samples within each group; **D.** Impact of comorbidities (see **Table S6**) on calprotectin plasma level within each group; **E.** Volcanoplot representation of cytokine levels in severe patients with and without comorbidities; **F.** Impact of bacterial infections on calprotectin plasma level within each group; **G-I.** Spearman correlations between calprotectin plasma level and neutrophil count (**G)**, fibrinogen (**H)**, and D-dimers (**I)**; **J-L.** Spearman correlations between IL-6 plasma level and neutrophil count (**J)**, fibrinogen (**K)**, and D-dimers (**L)**. Wilcoxon rank-sum test, * P<0.05; ** P <0.01; *** P<0.001; **** P<0.0001; ns, non-significant.

Figure 6. Validation of severe COVID-19 innate immune signature. A. Spectral flow pipeline. **B.** Fraction of B cells, CD4^{+} T cells, CD8^{+} T cells and NK cells among total cells in individual samples (circles) within each group; **C.** Fraction of neutrophils in individual samples within each group; **D.** Neutrophil subsets identified by CD101 and CD10 expression within each

group (pooled data); **E**. Fraction of $CD10^{Low}CD101^{-}$ neutrophils among total neutrophils in individual samples within each group; **F**. Fraction of $CXCR4^{+}$ neutrophils among $CD10^{Low}CD101^{-}$ neutrophils as in E; **G.** Spearman correlation of time spent in ICU and non-classical monocyte fraction among total monocytes; patients with a bacterial infection as red dots; mean time spent in ICU, 5.46 days in patients with a low (≤5%) and 8.83 days in those with a high (>5%) $CD14^{low}CD16^{High}$ monocyte fraction; **H.** Fraction of classical monocytes among white blood cells in each individual sample within each group; **I.** Fraction of non-classical monocytes among total monocytes as in H; **J**. Monocyte subset partition within each group (pooled data), the severe group being split in two groups, based on mean time spent in ICU; upper panel, monocyte subsets identified by CD14 and CD16 expression; lower panels, HLA-DR and CD169 or CD11b and CD141 expression on classical monocyte subset; **K.** Fractiob of monocytes expressing CD169 among classical monocytes as in H; **L.** Fraction of monocytes expressing CD141 among classical monocytes as in H; Kruskal-Wallis test, * P<0.05; ** P <0.01; *** P<0.001; ns, non-significant.

Figure 7. Low dimensional flow analysis of non-classical monocyte subsets in COVID-19. A. Fraction of $CD10^{Lcow}CD101^{-}$ neutrophils among total neutrophils in individual samples within each group, separating moderate and severe COVID-19; **B.** Calprotectin plasma level in moderate (orange dots) compared to patients of the three other groups; **C.** Fraction of non-classical monocytes among total monocytes in moderate (green bar plot) compared to patients of the three other three groups; **D-E.** Fraction of non-classical monocytes among total monocytes in a learning cohort of 98 patients (controls, n=56; mild, n=16; moderate, n=10; severe, n =16) (**D)** and a validation cohort of 24 patients (controls, n=10; mild n=3; moderate n=4, severe n=7) (**E)**; * Mann Whitney test, * P<0.05; ** P <0.01; *** P<0.001; **F-M.** Integration of scRNAseq data from blood and lung (bronchoalveolar lavage fluid) cells in COVID-19 patients. Blood samples described in **Table S3 and S4**; lung data from Liao et al., (controls, n=3; mild n=3; severe n=6); **F.** UMAP analysis of integrated scRNAseq from blood and lung samples. **G.** UMAP analysis of blood and lung samples in each patient category; **H.** UMAP analysis of integrated scRNAseq data of monocytes/macrophages from blood and lung; **I.** UMAP analysis of blood and lung monocytes/macrophages in each patient group; **J.** Violin plot representation of gene expression in lung monocytes/macrophages of control, mild and severe patients; **K.** UMAP analysis of integrated scRNAseq data of neutrophils from blood and lung samples; **L.** UMAP analysis of blood and lung neutrophils in each patient group. **M.** Violin plot representation of gene expression in lung neutrophils of control, mild and severe COVID-19 patients; **N.** UMAP analysis of neutrophils with *CXCR4* gene expression level projection (low expression = grey dots; high expression = dark blue dots).

Supplemental Figure titles and legends

Supplemental Figure 1. Related to Figure 1; Table S2. Spectral flow analysis of peripheral blood cells in a learning cohort of controls and COVID-19 patients. A. Representative example of data pooling of individual UMAP profiles obtained from 3 patients of the same group. Here, neutrophil subsets are identified based on CD10 and CD101 expression across cells from patients 1, 2 and 3, allowing the analysis of cell subset repartition within the group; **B.** Cell surface marker expression identifying cell populations on UMAP analysis generated by data pooling from all the tested samples; **C.** UMAP profile from pooled data on neutrophils in all patients or indicated group of patients; **D-E.** Percentage of $CD10^{High}$ (**D**) or $CD16^{Low}$ neutrophils (**E**) among total neutrophils in all individuals of indicated groups; **F.** UMAP profile from pooled data on monocytes in all patients or indicated group of patients; **G-H.** Percentage of $CD14^{+}$ (**G**) or $CD11b^{High}$ (**H**) monocytes among total monocytes in all individuals of indicated groups; Kruskal-Wallis test, * P<0.05; ** P <0.01; *** P<0.001; ns, non-significant.

Supplemental Figure 2. Related to Figure 2; Table S3-S4. Single cell analysis of peripheral blood cells. A. Heatmap of gene expression used to identify cell populations in scRNAseq experiments; **B-C.** Individual UMAP analysis of each control sample analyzed by scRNAseq **(B)** and spectral flow cytometry **(C)**.

Supplemental Figure 3. Related to Figure 3; Table S3-S5. Monocyte analysis by single cell RNA sequencing, spectral flow cytometry and mass cytometry. A. Pathway analysis generated by comparing DEGs in monocytes of each SARS-CoV-2 positive patient to the same population in the three control patients considered together using IPA software (mild patient in blue, severe #1 in red, severe # 2 in orange); **B.** The same DEGs were used to perform a gene ontology network analysis using clueGO software, considering the two severe patients together; **C.** Combined (left panel) and individual (right panel) mass cytometry analysis of p65/NF-κB expression in circulating $CD34^{+}$ cells in each group.

Supplemental Figure 4. Related to Figure 4; Table S3-S5. Neutrophil analysis by single cell RNA sequencing, spectral flow cytometry and mass cytometry. A. Heatmap of the top 20 DEGs defining two neutrophil clusters. **B.** Pathway analysis generated by comparing DEGs in neutrophils of each SARS-CoV-2 patient to the same population in the three control patients considered together using IPA software (mild patient in blue, severe #1 in red, severe # 2 in orange); **C.** The same DEGs identified in neutrophils were used to perform a gene ontology network analysis using clueGO software, considering the two severe patients together.

Supplemental Figure 5. Related to Figure 5; Table S5-S6. Calprotectin is the most abundant immune mediator/immune protein detected in the plasma of severe COVID-19 patients. A. RT-qPCR analysis of *S100A8* and *S100A9* gene expression in the three groups of patients,

using *HPRT* as a control gene; **B.** Heatmap of cytokines, chemokines, IFNα2a and calprotectin plasma levels in 37 COVID-19 patients compared to 40 controls. SARS-CoV-2-positive patients included 14 mild and 23 severe patients. Associated bacterial infection at sample collection is indicated in purple. The heatmap shows z score-normalized concentrations, each column represents one patient and each row one protein; the color gradient from blue to red indicates increasing concentrations. Rows and columns are clustered using correlation distance and average linkage; **C.** Volcano-plot representation of cytokine levels in severe SARS-CoV-2 patients with (n=11) or without (n=14) bacterial infection at the time of sample collection; **D.** Spearman correlation between calprotectin concentration and age showing control patients in green, mild in orange and severe in red; **E.** Spearman correlation between IL-6 and calprotectin concentrations (color code as in D).

Supplemental Figure 6. Related to Figure 6; Table S6. Validation of innate immune signature of severe COVID-19. A-B Non-supervised UMAP representation generated by pooling data from all the patient samples; cell identification (**A**) surface marker expression (**B**); **C.** Bar plots representing the percentage of $CD10^{Low}CD16^{Low}$ neutrophils among all neutrophils in individual patients from each group in the validation cohort (n=90). **D.** Spearman correlation between CD169 (*SIGLEC-1*) mean fluorescence intensity (MFI) and days spent by severe patients in ICU. **E.** Spearman correlation between CD169 (*SIGLEC-1*) mean fluorescence intensity (MFI) and plasma IFNα concentration; yellow, mild COVID-19 patients; red, severe COVID-19 patients. **F.G.** Bar plots representing the percentage of HLA-DR^{Low} classical monocytes, B cells, $CD4^+$ and $CD8^+$ T cells and NK cells (**F**) and neutrophils among $CD45^+$ cells, $CD10^{Low}CD101^-$ neutrophils among all neutrophils and $CD10^{Low}CXCR4^+$ neutrophils among $CD10^{Low}CD101^-$ neutrophils (**G**) in individual patients from each group in the validation cohort (n=90).

Supplemental Figure 7. Related to Figure 7; Table S6-S7. Changes in innate immune cell phenotype are detected in moderate COVID-19 patients. A. Bar plots representing the percentage of B cells, $CD4^+$ T cells, $CD8^+$ T cells, NK cells, total monocytes, $CD169^+$, HLA-DR^{Low} and $CD141^+$ classical monocyte subsets, total neutrophils among $CD45^+$ cells, and $CD10^{Low}CD101^-$ and $CD10^{Low}CD16^{Low}$ neutrophil subset among all neutrophils in individual patients from each group, with the moderate category (6 patients) highlighted. **B.** Plasma concentration of IFNα in moderate COVID-19 patients compared to the three other groups. **C.** ROC analysis showing performance of a diagnostic test using percentage of non-classical monocytes among total monocytes to distinguish controls and mild COVID patients from moderate and severe COVID patients**; D.** Monocyte subset analysis in the peripheral blood of 2 severe patients, before (left panels) and after (right panels) treatment with the indicated anti-IL-6 antibodies; **E.** Percentage of HLA-DR^{low} classical monocytes among classical monocytes in a cohort of 22 patients and 17 controls grouped into 4 clinical categories; **F.** Correlation between the percentage of HLA-DR^{low} classical monocytes and non-classical monocytes; **G.** Percentage of $CD16^{low}$ neutrophils among neutrophils in control and COVID-

19 patients of the learning cohort described in **Figure 7**. **H.** ROC curves evaluating the discriminating significance of calprotectin plasma level (yellow), nonclassical monocyte fraction (red), $CD16^{low}$ circulating neutrophils (blue) and IFNα2a plasma level (white) between controls/mild patients and moderate/severe patients. AUC, Area Under the Curve; Mann Whitney test; **I.** Heatmap of blood and bronchoalveolar lavage fluid scRNAseq cells integrated defining the 5 regions of cell populations; **J.** Pathway analysis (Cytoscape and ClueGo) of DEGs expressed at a higher level in bronchoalveolar monocytes/macrophages from mild versus severe patients. **K.** UMAP analysis of neutrophils with *S100A8* (left panel) and *S100A9* (right panel) gene expression level projection (low expression = grey dots; high expression = dark blue dots). * $P<0.05$; ** $P<0.01$; *** $P<0.001$.

STAR Methods text

RESSOURCE AVAILABILITY

Lead Contact. Further information and request for resources and reagents should be directed to and will be fulfilled by the lead contact: Florent_Ginhoux@immunol.a-star.edu.sg (F.Gi.)

Materials Availability Statement. This study did not generate new unique reagents.

Data and Code Availability. All blood scRNA-seq data used in this study can be accessed by ArrayExpress Archive of Functional Genomics Data under the accession number **E-MTAB-9221**. Integrated BALF scRNA-seq data can be accessed in GEO under the accession number **GSE145926**.
Additional Supplemental Items are available from Mendeley Data at http://dx.doi.org/10.17632/b6wvz54dxp.2

EXPERIMENTAL MODEL SUBJECT DETAILS

Patients. This non-interventional study was approved by institutional review boards of Cochin-Port Royal (Paris, France) and Gustave Roussy (Villejuif, France) hospitals and the ethical committee of Cochin-Port Royal Hospital (CLEP Decision N°: AAA-2020-08023), and conformed to the principles outlined in the Declaration of Helsinki. Controls (n = 72) were symptomatic patients who were seen at Hôtel-Dieu or Gustave Roussy COVID-19 screening unit and were negative for SARS-CoV-2 RT-PCR on pharyngeal swab. Mild COVID-19 patients (n = 27) were defined by having limited clinical symptoms (fever, cough, diarrhea, myalgia, anosmia/ageusia) that did not require CT-scan or hospitalization. Moderate cases (n = 16) were defined as symptomatic patients with dyspnea and radiological findings of pneumonia on thoracic CT scan, requiring hospitalization and a maximum of 9 L/min of oxygen. In the larger part of this study, mild and moderate cases were analyzed together and grouped under “mild category”. Severe patients (n = 43) were those hospitalized in the ICU with respiratory distress requiring 10L/min of oxygen or more, without or with endotracheal intubation and mechanical ventilation.

METHOD DETAILS

Sampling. Whole human peripheral blood was collected into sterile vacutainer tubes containing EDTA or heparin. Except for single cell RNA sequencing, tubes were centrifuged at 300 g for 5 min at room temperature and plasma was collected. Whole blood was mixed at a 1:1 ratio with Whole Blood Cell Stabilizer (Cytodelics), incubated at room temperature for 10 min and transferred to -80°C freezer to await analysis. These samples were secondarily

thawed in a water bath set to +37°C. Cells were fixed at a ratio 1:1 with Fixation Buffer (Cytodelics, ratio 1:1) and incubated for 10 min at room temperature. Red blood cells were lysed by addition of 2 mL of Lysis Buffer (Cytodelics, ratio 1:4) at room temperature for 10 min. White blood cells were washed with 2 mL of Wash Buffer (Cytodelics, ratio 1:5).

Spectral flow Cytometry. Cells were resuspended in 100 µL extra-cellular antibody cocktail and incubated at room temperature for 15 min. For intra-cellular labelling, a step of permeabilization was performed using 200 µL of BD Cytofix/Cytoperm Kit (BD); cells were then incubated for 40 min at +4°C, washed in Perm Buffer (BD) and resuspended in intra-cellular antibody cocktail. After incubation, cells were washed in Flow Cytometry Buffer (1% BSA, 0.5% Na-Azide and 0.5M EDTA in PBS) and resuspended to proceed to the acquisition. All antibodies are listed in **the Key Resource Table**. Samples were acquired on CyTEK Aurora flow cytometer (Cytek Biosciences). Fcs files were exported and analyzed using FlowJo software.

3' scRNAseq analysis of human blood cells. To fully capture peripheral blood cell heterogeneity, we analyzed fresh samples without cell sorting or freezing and without Ficoll enrichment, minimizing time of incubation and processing. Sample preparation was done at room temperature. After red cell lysis, single-cell suspensions were loaded onto a Chromium Single Cell Chip (10x Genomics) according to the manufacturer's instructions for co-encapsulation with barcoded Gel Beads at a target capture rate of ~7000 individual cells per sample. To analyze neutrophils, we added RNase inhibitor (RNAse OUT Recombinant Ribonuclease Inhibitor Invitrogen, 40U/mL) into the loading buffer. Captured mRNAs were barcoded during cDNA synthesis using the Chromium Single Cell 3' Solution v3 (10x Genomics) according to the manufacturer's instructions. Of note, we increased the PCR cycles by two during cDNA amplification. All samples (at Day 0 and Day 10) were processed simultaneously with the Chromium Controller (10x Genomics) and the resulting libraries were prepared in parallel in a single batch. We pooled all of the libraries for sequencing in a single SP Illumina flow cell. All of the libraries were sequenced with an 8-base index read, a 28-base Read1 containing cell-identifying barcodes and unique molecular identifiers (UMIs), and a 91-base Read2 containing transcript sequences on an Illumina NovaSeq 6000. Reads were aligned to the hg19 genome and were used for subsequent analysis.

Analysis of scRNAseq and integration of dataset from bronchoalveolar lavage fluid of COVID-19 patients. Using the package Seurat V3 (Stuart et al., 2019), we normalized and scaled scRNA sequencing data. We next applied a principle component analysis to the scRNA sequencing results yielding a number of significant PCs (Using Jackstraw plot analysis). In addition, the standard deviation differences from one PC to another was taken into account as described by the Seurat V3 manual (Struart et al., 2019). To generate UMAP plots, min_distance was set as 0.3 and n_neighbors was set to 30. By dimensionality reduction, distinct clusters were identified and described by performing the FindClusters feature. The resolution of this feature was reduced to 0.3 to identify main cellular population only. Following this, differential genes were identified by performing the FindAllMarkers function and selecting genes that were differentially expressed (logFC >/= +/- 0.25 and FDR < 0.05). This approach identified a number of well characterized blood cell populations. Clustering and analysis of specific cell populations were performed in a similar manner to as previously

stated. Cells were clustered and separated based on well described markers (CD14/CD16 as describing monocyte populations).

The bronchoalveolar dataset was downloaded from the NIH GEO database (Liao et al., dataset GSE145926) and integrated with our own blood scRNAseq data using the Seurat V3 anchoring method (Stuart et al., 2019). Briefly, the datasets were normalized independently and the highly variable genes were identified for each dataset using the Seurat pipeline. A corrected data matrix with both datasets was then generated using the Seurat v3 anchoring procedure to allow for joint analysis. The matrix was scaled and a Principal Component Analysis (PCA) was performed using the Seurat v3 pipeline. A UMAP was performed on the 30 first Principal Components (PCs) (Becht et al., 2018). These principle components and subsequent clustering and analysis of scRNA sequencing data was performed as previously described.

Comparisons between patient samples were performed by a variation of the FindMarkers function that compared the differentially expressed genes from different samples, patient groups, and organs. Cutoff values were determined as previously described.

RT-qPCR analysis. Total RNA was extracted with RNeasy Mini Kit (Qiagen) and reverse transcribed with SuperScript™ IV VILO™ Master Mix with ezDNase™ Enzyme (Invitrogen). Real-time quantitative polymerase chain reaction (RT-qPCR) was performed using Power SYBR™ Green PCR Master Mix in a BioRad CFX96 thermocycler using the standard SyBR Green detection protocol as outlined by the manufacturer (Applied Biosystems). Briefly, 12 ng of total cDNA, 50nM (each) primers and 1× SyBR Green mixture were used in a total volume of 20 µL. Human primer sequences are the following: GUS (F: GAAAATATGTGGTTGGAGAGCTCATT; R: CCGAGTGAAGATCCCCT TTTTA); HPRT (F: GGACAGGACTGAACGTCTTGC; R: CTTGAGCACACAGAGGGCTACA); S100A8 (F: CAACACTG ATGGTGCAGTTAACTTC; R: CTGCCACGCCCATCTTTATC); S100A9 (F: CTGAGCTTCGAGG AGTTCATCA; R: CGTCACCCTCGTGCATCTTC).

Cytokine and chemokine measurements. Plasma samples (**Supplemental Table 6**) were centrifuged for 15 min at 1,000 g, diluted 1:4, then monitored using the Bio-Plex Pro™ Human Chemokine Panel 40-plex Assay (Bio-rad, ref: 171AK99MR2) according to the manufacturer's instructions. 40-plex cytokines and chemokines provided are: CCL1, CCL11, CCL13, CCL15, CCL17, CCL19, CCL2, CCL20, CCL21, CCL22, CCL23, CCL24, CCL25, CCL26, CCL27, CCL3, CCL7, CCL8, CX3CL1, CXCL1, CXCL10, CXCL11, CXCL12, CXCL13, CXCL16, CXCL2, CXCL5, CXCL6, CXCL8, CXCL9, GM-CSF, IFNα, IL-10, IL-16, IL-1b, IL-2, IL-4, IL-6, MIF, TNFa. Acquisitions and analyses were performed on a Bio-Plex 200 system (Bio-rad) and a Bio-Plex Manager 6.1 Software (Bio-rad), respectively. Soluble Calprotectin (diluted 1:100) and IFNα2a were analyzed using a R-plex Human Calprotectin Antibody Set (Meso Scale Discovery, ref: F21YB-3) and the ultra-sensitive assay S-plex Human IFNα2a kit (Meso Scale Discovery, ref: K151P3S-1), respectively, following manufacturer's instructions. Acquisitions and analyses of soluble Calprotectin and IFNα were performed on a MESO™ QuickPlex SQ120 reader and the MSD's Discovery Workbench 4.0. Each plasma sample was assayed twice with the average value taken as the final result. Data representation was performed with software R v3.3.3 using tidyverse, dplyr, ggplot2, ggpubr, pheatmap, corrplot or Hmisc packages.

Mass Cytometry. Cells were barcoded using the 20-Plex Pd barcoding kit (Fluidigm). Briefly, they were washed in Barcode Perm Buffer, resuspended in 800 µL of Barcode Perm Buffer

and 100 µL of each barcode were transferred to the appropriate sample. Cell suspensions were incubated for 30 min at room temperature, washed twice with Cell Staining Buffer (Fluidigm) and pooled, suspended in 100 µL filtered antibody cocktail, and incubated for 30 min at +4°C. All antibodies used are listed in **Key Resource Table**. After staining, cells were washed with Cell Staining Buffer and permeabilized with 200 µL of Fix/Perm from Foxp3/Transcription Factor Staining Buffer kit (eBiosciences), 40 min at +4°C. After incubation, cells were washed in Perm Buffer from Foxp3/Transcription Factor Staining Buffer kit (eBiosciences), resuspended in 100 µL filtered antibody cocktail, incubated for 30 min at +4°C, washed in Cell Staining Buffer and resuspended in 50 µL of CytoFix/Perm for 5 min at room temperature. Then, 400 µL of PBS containing 1.6% PFA + Iridium (1:4000) were added for 35 min at room temperature. Finally, cells were washed in Cell Staining Buffer, resuspended in 50 µL and stored at +4°C until acquisition. Cells were counted, washed and resuspended in Maxpar Cell Acquisition Solution at 0.5x 10^6 / mL and mixed with 10% EQ Beads immediately before acquisition on Helios mass cytometer using noise reduction, event length limits of 10-150 pushes. An average of 500,000 events were acquired per sample at a flow rate of 0.03mL/min. Mass cytometry standard files were normalized to a global standard determined for each log of EQ beads using CyTOF Software v.6.7.1014 (Fluidigm). Fcs files were exported and analysed using FlowJo software. UMAP was performed with n_neighbours of 15 and a min_distance of 0.2. Clusters were identified by the detection of commonly used cell markers (T cells expressing CD4 or CD8, neutrophils expressing CD15, and monocytes expressing CD14 and or CD16).

Routine multiparameter flow analysis test. Whole-blood samples (200µL) were labelled with anti-CD14-PC7 (clone RMO52); CD16-PB (clone 3G8); CD2-FITC (clone 39C1.5); CD56-PC5.5 (clone N901); CD24-PE (clone ALB9); CD45-KO (clone J33) and HLA-DR-APC (clone Immu-357) antibodies, all purchased from Beckman-Coulter. Red blood cells were lysed with 1 mL VersalyseTM (Beckman Coulter) before sample analysis with a Navios Cytometer (Beckman Coulter) as described (Tarfi et al., 2019). Monocytes were selected as $CD45^{High}/SSC^{Int}$ cells among living cells and singlets before excluding T cells as $CD2^{+}/SSC^{Low}$, NK cells as $CD56^{+}/SSC^{Low/Int}$, B cells as $CD24^{+}/SSC^{Low}$, immature and mature granulocytes as $CD24^{+}/SSC^{Int/High}$, $CD16^{Bright}$ residual granulocytes, and remaining $CD14^{-}CD16^{-}$ cells corresponding mainly to basophils and NK cells not previously excluded. Monocyte subsets were detected on a CD45/SCC dot plot, using a CD14/CD16 scattergram that separates $CD14^{High}CD16^{Low}$ (classical), $CD14^{High}/CD16^{High}$ (intermediate) and $CD14^{Low}CD16^{High}$ (non-classical) subsets. Finally, the proportion of monocytes HLA-DR^{Low} was evaluated on a HLA-DR/CD14 scattergram.

QUANTIFICATION AND STATISTICAL ANALYSIS

Data analysis. Calculations and statistical tests were performed using R v3.3.3. Unless stated, p-values are two-sided with 95% confidence intervals for the reported statistic of interest. Individual data points representing the measurement from one patient are systematically calculated from the corresponding distribution. Wilcoxon rank-sum test was applied to assess differences in concentration between two different groups. When indicated, the false discovery rate (FDR, $p > 0.05$) was controlled using the Benjamini–Hochberg procedure. Spearman correlations were computed using Hmisc R package and cytokine results were shown using R package Pheatmap. Soluble factor fold ratios were

calculated as log2 transformation of values of mild and severe patients versus median value of all control patients, and were converted to z scores. Hierarchical clustering of the patients based on the z score of 42 soluble factors was performed using euclidean distance and ward.D clustering. Gene ontology networks were made by subjecting the DEGs from previous scRNA sequencing analysis to the Cytoscape addon ClueGO. The selected DEGs were specific to those with increased expression by monocytes and neutrophils from mild or severe SARS-CoV-2 positive patients. Biological Process gene ontologies selected had an FDR < 0.05. Other statistical analyses were performed using GraphPad Prism 7.

A generalized linear model was also used to analyze interactions between biological parameters. First, neutrophil count, calprotectin, fibrinogen, IL-6 and D-dimers were normalized using log transformation. Then, calprotectin plasma level was modeled using multivariable linear regression adjusted for the other parameters, and their interaction with the groups. Similar approach was performed to model IL-6. Backward selection was applied to obtain a parsimonious model.

To identify the most discriminant markers, we used a logistic regression adjusted for the scaled log2-transformed markers. Parameters were penalized using the least absolute shrinkage and selection operator (lasso) to limit overfitting due to the high number of markers. The regularization parameter was selected from 10 folds cross-validation using the glmnet R package (Friedman et al., 2010). The final AUC estimate was corrected for optimism using the Harrell's method (Harrell et al., 1996), and its confidence interval was computed using the two-stage approach proposed by Noma et al (Noma et al., 2020) with 2000 bootstrap samples for each stage. In this analysis, we included age, sex and comorbidities together with biological parameters. Given the absence of validation cohort, AUC was corrected to limit overfitting bias. This correction indicated an AUC at 99.7% (95% confidence interval [98.8%; 100.0%]). The final score corresponds to the following equation:

$$Score = \frac{1}{1 + \exp(0.272 - 1.530\ C_1 - 0.013\ \ C_2 - 0.216\ \ C_3 - \ 0.212\ C_4)}$$

With C_1, C_2, C_3, and C_4, the values of the calprotectin, CX3CL1, CXCL11 and CXCL13 which are log2 transformed and scaled according to the value training cohort: $C_1 = \frac{log2(C\text{alprotectin})\text{-}19.285}{2.278}$, $C_2 = \frac{log2(CX3CL1)\text{-}7.803}{0.892}$, $C_3 = \frac{log2(CXCL11)\text{-}5.503}{1.691}$, and $C_4 = \frac{log2(CXCL13)\text{-}5.189}{1.372}$.

ADDITIONAL RESSOURCES

Table S4 related to Figures 2-4; Figures S2-4: Excel sheet providing the detailed results of scRNA seq experiments shown on Figure 2 to 4, including metadata, cell population numbers, cell population differentially expressed genes (DEGs), monocyte DEGs and neutrophils DEGs.

References

Aarts, C.E.M., Hiemstra, I.H., Beguin, E.P., Hoogendijk, A.J., Bouchmal, S., van Houdt, M., Tool, A.T.J., Mul, E., Jansen, M.H., Janssen, H., et al. (2019). Activated neutrophils exert myeloid-derived suppressor cell activity damaging T cells beyond repair. Blood Adv 3, 3562-3574.

Al-Qahtani, A.A., Lyroni, K., Aznaourova, M., Tseliou, M., Al-Anazi, M.R., Al-Ahdal, M.N., Alkahtani, S., Sourvinos, G., and Tsatsanis, C. (2017). Middle east respiratory syndrome corona virus spike glycoprotein suppresses macrophage responses via DPP4-mediated induction of IRAK-M and PPARgamma. Oncotarget 8, 9053-9066.

Austermann, J., Friesenhagen, J., Fassl, S.K., Petersen, B., Ortkras, T., Burgmann, J., Barczyk-Kahlert, K., Faist, E., Zedler, S., Pirr, S., et al. (2014). Alarmins MRP8 and MRP14 induce stress tolerance in phagocytes under sterile inflammatory conditions. Cell Rep 9, 2112-2123.

Basiorka, A.A., McGraw, K.L., Eksioglu, E.A., Chen, X., Johnson, J., Zhang, L., Zhang, Q., Irvine, B.A., Cluzeau, T., Sallman, D.A., et al. (2016). The NLRP3 inflammasome functions as a driver of the myelodysplastic syndrome phenotype. Blood 128, 2960-2975.

Becht, E., McInnes, L., Healy, J., Dutertre, C.A., Kwok, I.W.H., Ng, L.G., Ginhoux, F., and Newell, E.W. (2018). Dimensionality reduction for visualizing single-cell data using UMAP. Nat Biotechnol.

Bost, P., Giladi, A., Liu, Y., Bendjelal, Y., Xu, G., David, E., Blecher-Gonen, R., Cohen, M., Medaglia, C., Li, H., et al. (2020). Host-Viral Infection Maps Reveal Signatures of Severe COVID-19 Patients. Cell.

Channappanavar, R., Fehr, A.R., Zheng, J., Wohlford-Lenane, C., Abrahante, J.E., Mack, M., Sompallae, R., McCray, P.B., Jr., Meyerholz, D.K., and Perlman, S. (2019). IFN-I response timing relative to virus replication determines MERS coronavirus infection outcomes. J Clin Invest 130, 3625-3639.

Chen, G., Wu, D., Guo, W., Cao, Y., Huang, D., Wang, H., Wang, T., Zhang, X., Chen, H., Yu, H., et al. (2020a). Clinical and immunological features of severe and moderate coronavirus disease 2019. J Clin Invest 130, 2620-2629.

Chen, L., Long, X., Xu, Q., Tan, J., Wang, G., Cao, Y., Wei, J., Luo, H., Zhu, H., Huang, L., et al. (2020b). Elevated serum levels of S100A8/A9 and HMGB1 at hospital admission are correlated with inferior clinical outcomes in COVID-19 patients. Cell Mol Immunol.

Chen, N., Zhou, M., Dong, X., Qu, J., Gong, F., Han, Y., Qiu, Y., Wang, J., Liu, Y., Wei, Y., et al. (2020c). Epidemiological and clinical characteristics of 99 cases of 2019 novel coronavirus pneumonia in Wuhan, China: a descriptive study. Lancet 395, 507-513.

Chen, X., Bracht, J.R., Goldman, A.D., Dolzhenko, E., Clay, D.M., Swart, E.C., Perlman, D.H., Doak, T.G., Stuart, A., Amemiya, C.T., et al. (2014). The architecture of a scrambled genome reveals massive levels of genomic rearrangement during development. Cell 158, 1187-1198.

Chen, X., Eksioglu, E.A., Zhou, J., Zhang, L., Djeu, J., Fortenbery, N., Epling-Burnette, P., Van Bijnen, S., Dolstra, H., Cannon, J., et al. (2013). Induction of myelodysplasia by myeloid-derived suppressor cells. J Clin Invest 123, 4595-4611.

Chu, H., Chan, J.F., Wang, Y., Yuen, T.T., Chai, Y., Hou, Y., Shuai, H., Yang, D., Hu, B., Huang, X., et al. (2020). Comparative replication and immune activation profiles of SARS-CoV-2 and SARS-CoV in human lungs: an ex vivo study with implications for the pathogenesis of COVID-19. Clin Infect Dis.

Desforges, M., Miletti, T.C., Gagnon, M., and Talbot, P.J. (2007). Activation of human monocytes after infection by human coronavirus 229E. Virus Res 130, 228-240.

Dobin, A., Davis, C.A., Schlesinger, F., Drenkow, J., Zaleski, C., Jha, S., Batut, P., Chaisson, M., and Gingeras, T.R. (2013). STAR: ultrafast universal RNA-seq aligner. Bioinformatics 29, 15-21.

Eksioglu, E.A., Chen, X., Heider, K.H., Rueter, B., McGraw, K.L., Basiorka, A.A., Wei, M., Burnette, A., Cheng, P., Lancet, J., et al. (2017). Novel therapeutic approach to improve hematopoiesis in low risk MDS by targeting MDSCs with the Fc-engineered CD33 antibody BI 836858. Leukemia 31, 2172-2180.

Evrard, M., Kwok, I.W.H., Chong, S.Z., Teng, K.W.W., Becht, E., Chen, J., Sieow, J.L., Penny, H.L., Ching, G.C., Devi, S., et al. (2018). Developmental Analysis of Bone Marrow Neutrophils Reveals Populations Specialized in Expansion, Trafficking, and Effector Functions. Immunity 48, 364-379 e368.

Fassl, S.K., Austermann, J., Papantonopoulou, O., Riemenschneider, M., Xue, J., Bertheloot, D., Freise, N., Spiekermann, C., Witten, A., Viemann, D., et al. (2015). Transcriptome assessment reveals a dominant role for TLR4 in the activation of human monocytes by the alarmin MRP8. J Immunol 194, 575-583.

Fizazi, K., Ulys, A., Sengelov, L., Moe, M., Ladoire, S., Thiery-Vuillemin, A., Flechon, A., Guida, A., Bellmunt, J., Climent, M.A., et al. (2017). A randomized, double-blind, placebo-controlled phase II study of maintenance therapy with tasquinimod in patients with metastatic castration-resistant prostate cancer responsive to or stabilized during first-line docetaxel chemotherapy. Ann Oncol 28, 2741-2746.

Freise, N., Burghard, A., Ortkras, T., Daber, N., Imam Chasan, A., Jauch, S.L., Fehler, O., Hillebrand, J., Schakaki, M., Rojas, J., et al. (2019). Signaling mechanisms inducing hyporesponsiveness of phagocytes during systemic inflammation. Blood 134, 134-146.

Furman, D., Campisi, J., Verdin, E., Carrera-Bastos, P., Targ, S., Franceschi, C., Ferrucci, L., Gilroy, D.W., Fasano, A., Miller, G.W., et al. (2019). Chronic inflammation in the etiology of disease across the life span. Nat Med 25, 1822-1832.

Giamarellos-Bourboulis, E.J., Netea, M.G., Rovina, N., Akinosoglou, K., Antoniadou, A., Antonakos, N., Damoraki, G., Gkavogianni, T., Adami, M.E., Katsaounou, P., et al. (2020). Complex Immune Dysregulation in COVID-19 Patients with Severe Respiratory Failure. Cell Host Microbe.

Gordon, D.E., Jang, G.M., Bouhaddou, M., Xu, J., Obernier, K., White, K.M., O'Meara, M.J., Rezelj, V.V., Guo, J.Z., Swaney, D.L., et al. (2020). A SARS-CoV-2 protein interaction map reveals targets for drug repurposing. Nature.

Guan, W.J., and Zhong, N.S. (2020). Clinical Characteristics of Covid-19 in China. Reply. N Engl J Med 382, 1861-1862.

Guilliams, M., Mildner, A., and Yona, S. (2018). Developmental and Functional Heterogeneity of Monocytes. Immunity 49, 595-613.

Hadjadj, J., Yatim, N., Barnabei, L., Corneau, A., Boussier, J., Pere, H., Charbit, B., Bondet, V., Chenevier-Gobeaux, C., Breillat, P., et al. (2020). Impaired type I interferon activity and exacerbated inflammatory responses in severe Covid-19 patients. medRxiv, 2020.2004.2019.20068015.

Hajian-Tilaki, K. (2013). Receiver Operating Characteristic (ROC) Curve Analysis for Medical Diagnostic Test Evaluation. Caspian J Intern Med 4, 627-635.

Hanna, R.N., Carlin, L.M., Hubbeling, H.G., Nackiewicz, D., Green, A.M., Punt, J.A., Geissmann, F., and Hedrick, C.C. (2011). The transcription factor NR4A1 (Nur77) controls bone marrow differentiation and the survival of Ly6C- monocytes. Nat Immunol 12, 778-785.

Hofer, T.P., Zawada, A.M., Frankenberger, M., Skokann, K., Satzl, A.A., Gesierich, W., Schuberth, M., Levin, J., Danek, A., Rotter, B., et al. (2015). slan-defined subsets of CD16-positive monocytes: impact of granulomatous inflammation and M-CSF receptor mutation. Blood 126, 2601-2610.

Huang, C., Wang, Y., Li, X., Ren, L., Zhao, J., Hu, Y., Zhang, L., Fan, G., Xu, J., Gu, X., et al. (2020). Clinical features of patients infected with 2019 novel coronavirus in Wuhan, China. Lancet 395, 497-506.

Kraakman, M.J., Lee, M.K., Al-Sharea, A., Dragoljevic, D., Barrett, T.J., Montenont, E., Basu, D., Heywood, S., Kammoun, H.L., Flynn, M., et al. (2017). Neutrophil-derived S100 calcium-binding proteins A8/A9 promote reticulated thrombocytosis and atherogenesis in diabetes. J Clin Invest 127, 2133-2147.

Kramer, A., Green, J., Pollard, J., Jr., and Tugendreich, S. (2014). Causal analysis approaches in Ingenuity Pathway Analysis. Bioinformatics 30, 523-530.

Kratofil, R.M., Kubes, P., and Deniset, J.F. (2017). Monocyte Conversion During Inflammation and Injury. Arterioscler Thromb Vasc Biol 37, 35-42.

Kuipers, M.T., Vogl, T., Aslami, H., Jongsma, G., van den Berg, E., Vlaar, A.P., Roelofs, J.J., Juffermans, N.P., Schultz, M.J., van der Poll, T., et al. (2013). High levels of S100A8/A9 proteins aggravate ventilator-induced lung injury via TLR4 signaling. PLoS One 8, e68694.

Lefrancais, E., Ortiz-Munoz, G., Caudrillier, A., Mallavia, B., Liu, F., Sayah, D.M., Thornton, E.E., Headley, M.B., David, T., Coughlin, S.R., et al. (2017). The lung is a site of platelet biogenesis and a reservoir for haematopoietic progenitors. Nature 544, 105-109.

Li, H., Liu, L., Zhang, D., Xu, J., Dai, H., Tang, N., Su, X., and Cao, B. (2020). SARS-CoV-2 and viral sepsis: observations and hypotheses. Lancet 395, 1517-1520.

Liao, M., Liu, Y., Yuan, J., Wen, Y., Xu, G., Zhao, J., Cheng, L., Li, J., Wang, X., Wang, F., et al. (2020). Single-cell landscape of bronchoalveolar immune cells in patients with COVID-19. Nat Med.

Llitjos, J.F., Leclerc, M., Chochois, C., Monsallier, J.M., Ramakers, M., Auvray, M., and Merouani, K. (2020). High incidence of venous thromboembolic events in anticoagulated severe COVID-19 patients. J Thromb Haemost.

Lukaszewicz, A.C., Grienay, M., Resche-Rigon, M., Pirracchio, R., Faivre, V., Boval, B., and Payen, D. (2009). Monocytic HLA-DR expression in intensive care patients: interest for prognosis and secondary infection prediction. Crit Care Med 37, 2746-2752.

Mastio, J., Condamine, T., Dominguez, G., Kossenkov, A.V., Donthireddy, L., Veglia, F., Lin, C., Wang, F., Fu, S., Zhou, J., et al. (2019). Identification of monocyte-like precursors of granulocytes in cancer as a mechanism for accumulation of PMN-MDSCs. J Exp Med 216, 2150-2169.

Michot, J.M., Albiges, L., Chaput, N., Saada, V., Pommeret, F., Griscelli, F., Balleyguier, C., Besse, B., Marabelle, A., Netzer, F., et al. (2020). Tocilizumab, an anti-IL6 receptor antibody, to treat Covid-19-related respiratory failure: a case report. Ann Oncol.

Ng, L.G., Ostuni, R., and Hidalgo, A. (2019). Heterogeneity of neutrophils. Nat Rev Immunol 19, 255-265.

Nottet, H.S., Persidsky, Y., Sasseville, V.G., Nukuna, A.N., Bock, P., Zhai, Q.H., Sharer, L.R., McComb, R.D., Swindells, S., Soderland, C., et al. (1996). Mechanisms for the transendothelial migration of HIV-1-infected monocytes into brain. J Immunol 156, 1284-1295.

Patnaik, M.M., Sallman, D.A., Mangaonkar, A., Heuer, R., Hirvela, J., Zblewski, D., Al-Kali, A., Binder, M., Balasis, M.E., Newman, H., et al. (2020). Phase 1 study of lenzilumab, a recombinant anti-human GM-CSF antibody, for chronic myelomonocytic leukemia (CMML). Blood.

Raquil, M.A., Anceriz, N., Rouleau, P., and Tessier, P.A. (2008). Blockade of antimicrobial proteins S100A8 and S100A9 inhibits phagocyte migration to the alveoli in streptococcal pneumonia. J Immunol 180, 3366-3374.

Richardson, S., Hirsch, J.S., Narasimhan, M., Crawford, J.M., McGinn, T., Davidson, K.W., and the Northwell, C.-R.C., Barnaby, D.P., Becker, L.B., Chelico, J.D., et al. (2020). Presenting Characteristics, Comorbidities, and Outcomes Among 5700 Patients Hospitalized With COVID-19 in the New York City Area. JAMA.

Riva, M., Kallberg, E., Bjork, P., Hancz, D., Vogl, T., Roth, J., Ivars, F., and Leanderson, T. (2012). Induction of nuclear factor-kappaB responses by the S100A9 protein is Toll-like receptor-4-dependent. Immunology 137, 172-182.

Selimoglu-Buet, D., Riviere, J., Ghamlouch, H., Bencheikh, L., Lacout, C., Morabito, M., Diop, M., Meurice, G., Breckler, M., Chauveau, A., et al. (2018). A miR-150/TET3 pathway regulates the generation of mouse and human non-classical monocyte subset. Nat Commun 9, 5455.

Sevelsted, A., Stokholm, J., Bonnelykke, K., and Bisgaard, H. (2015). Cesarean section and chronic immune disorders. Pediatrics 135, e92-98.

Shannon, P., Markiel, A., Ozier, O., Baliga, N.S., Wang, J.T., Ramage, D., Amin, N., Schwikowski, B., and Ideker, T. (2003). Cytoscape: a software environment for integrated models of biomolecular interaction networks. Genome Res 13, 2498-2504.

Simard, J.C., Noel, C., Tessier, P.A., and Girard, D. (2014). Human S100A9 potentiates IL-8 production in response to GM-CSF or fMLP via activation of a different set of transcription factors in neutrophils. FEBS Lett 588, 2141-2146.

Smith, M.S., Bentz, G.L., Alexander, J.S., and Yurochko, A.D. (2004). Human cytomegalovirus induces monocyte differentiation and migration as a strategy for dissemination and persistence. J Virol 78, 4444-4453.

Stuart, T., Butler, A., Hoffman, P., Hafemeister, C., Papalexi, E., Mauck, W.M., 3rd, Hao, Y., Stoeckius, M., Smibert, P., and Satija, R. (2019). Comprehensive Integration of Single-Cell Data. Cell 177, 1888-1902 e1821.

Tarfi, S., Badaoui, B., Freynet, N., Morabito, M., Lafosse, J., Toma, A., Etienne, G., Micol, J.B., Sloma, I., Fenaux, P., et al. (2019). Disappearance of slan-positive non-classical monocytes for diagnosis of chronic myelomonocytic leukemia with associated inflammatory state. Haematologica.

Teran-Cabanillas, E., and Hernandez, J. (2017). Role of Leptin and SOCS3 in Inhibiting the Type I Interferon Response During Obesity. Inflammation 40, 58-67.

Thevarajan, I., Nguyen, T.H.O., Koutsakos, M., Druce, J., Caly, L., van de Sandt, C.E., Jia, X., Nicholson, S., Catton, M., Cowie, B., et al. (2020). Breadth of concomitant immune responses prior to patient recovery: a case report of non-severe COVID-19. Nat Med 26, 453-455.

Totura, A.L., and Baric, R.S. (2012). SARS coronavirus pathogenesis: host innate immune responses and viral antagonism of interferon. Curr Opin Virol 2, 264-275.

Ulas, T., Pirr, S., Fehlhaber, B., Bickes, M.S., Loof, T.G., Vogl, T., Mellinger, L., Heinemann, A.S., Burgmann, J., Schoning, J., et al. (2017). S100-alarmin-induced innate immune programming protects newborn infants from sepsis. Nat Immunol 18, 622-632.

Vabret, N., Samstein, R., Fernandez, N., Merad, M., Sinai Immunology Review, P., Trainees, and Faculty (2020). Advancing scientific knowledge in times of pandemics. Nat Rev Immunol 20, 338.

Veglia, F., Perego, M., and Gabrilovich, D. (2018). Myeloid-derived suppressor cells coming of age. Nat Immunol 19, 108-119.

Vogl, T., Stratis, A., Wixler, V., Voller, T., Thurainayagam, S., Jorch, S.K., Zenker, S., Dreiling, A., Chakraborty, D., Frohling, M., et al. (2018). Autoinhibitory regulation of S100A8/S100A9 alarmin activity locally restricts sterile inflammation. J Clin Invest 128, 1852-1866.

Walter, R.B. (2018). Investigational CD33-targeted therapeutics for acute myeloid leukemia. Expert Opin Investig Drugs 27, 339-348.

Wang, S., Song, R., Wang, Z., Jing, Z., Wang, S., and Ma, J. (2018). S100A8/A9 in Inflammation. Front Immunol 9, 1298.

Wang, T., Du, Z., Zhu, F., Cao, Z., An, Y., Gao, Y., and Jiang, B. (2020). Comorbidities and multi-organ injuries in the treatment of COVID-19. Lancet 395, e52.

Wilk, A.J., Rustagi, A., Zhao, N.Q., Roque, J., Martinez-Colon, G.J., McKechnie, J.L., Ivison, G.T., Ranganath, T., Vergara, R., Hollis, T., et al. (2020). A single-cell atlas of the peripheral immune response in patients with severe COVID-19. Nat Med 26, 1070-1076.

Yang, Y., Ye, F., Zhu, N., Wang, W., Deng, Y., Zhao, Z., and Tan, W. (2015). Middle East respiratory syndrome coronavirus ORF4b protein inhibits type I interferon production through both cytoplasmic and nuclear targets. Sci Rep 5, 17554.

Yilla, M., Harcourt, B.H., Hickman, C.J., McGrew, M., Tamin, A., Goldsmith, C.S., Bellini, W.J., and Anderson, L.J. (2005). SARS-coronavirus replication in human peripheral monocytes/macrophages. Virus Res 107, 93-101.

Silvin A et al, Figure 1

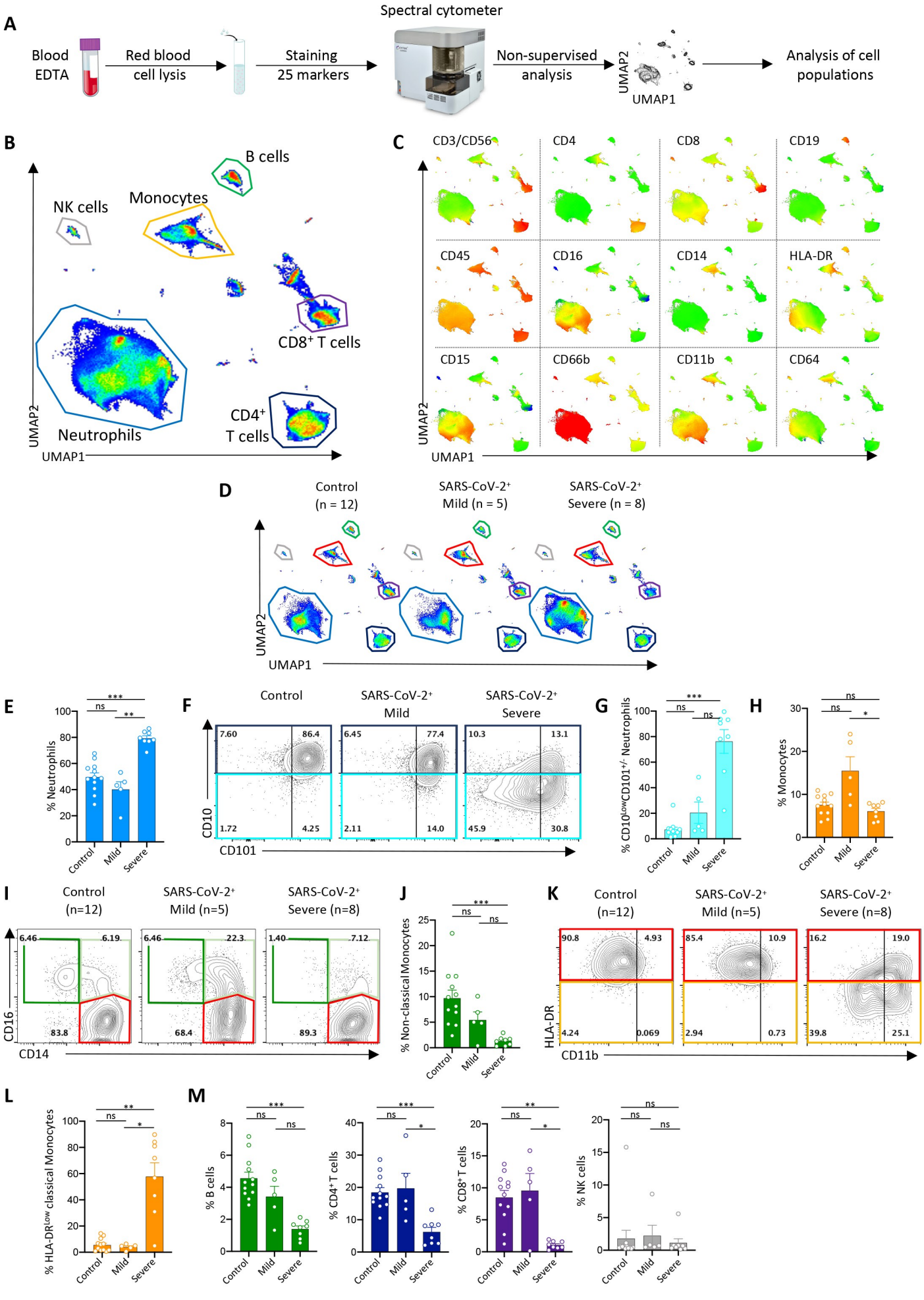

Silvin A et al, Figure 2

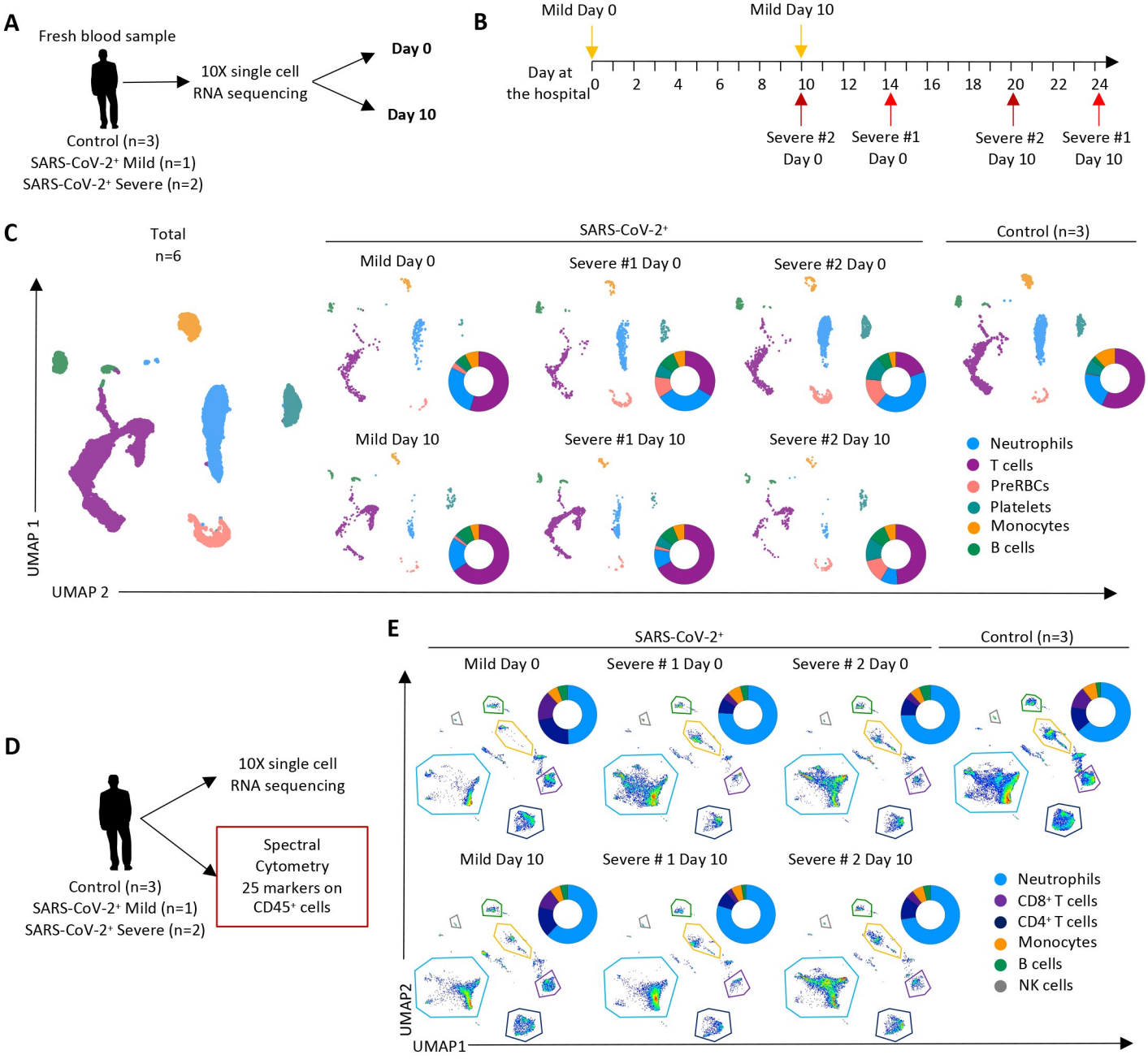

Silvin A et al, Figure 3

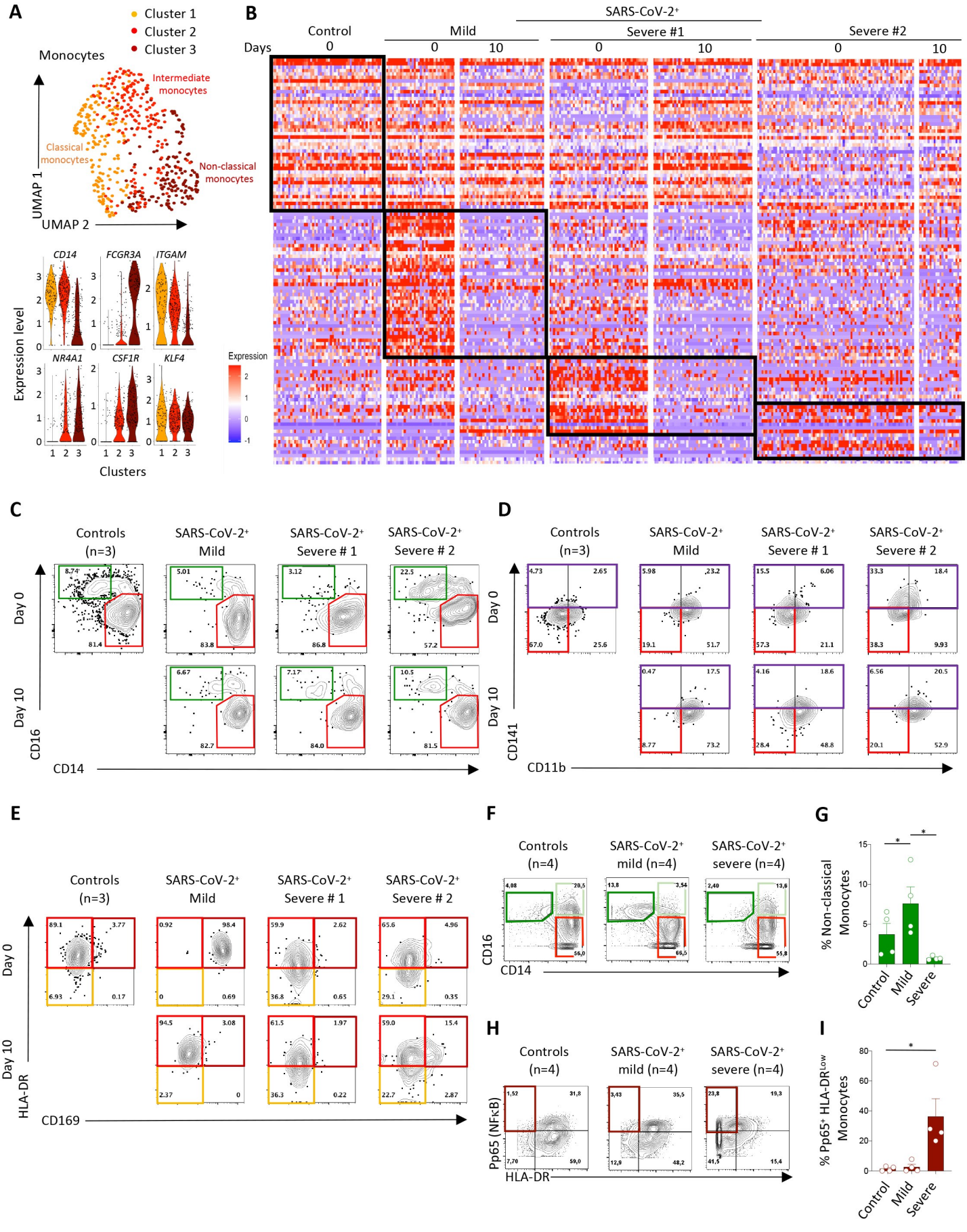

Silvin A et al, Figure 4

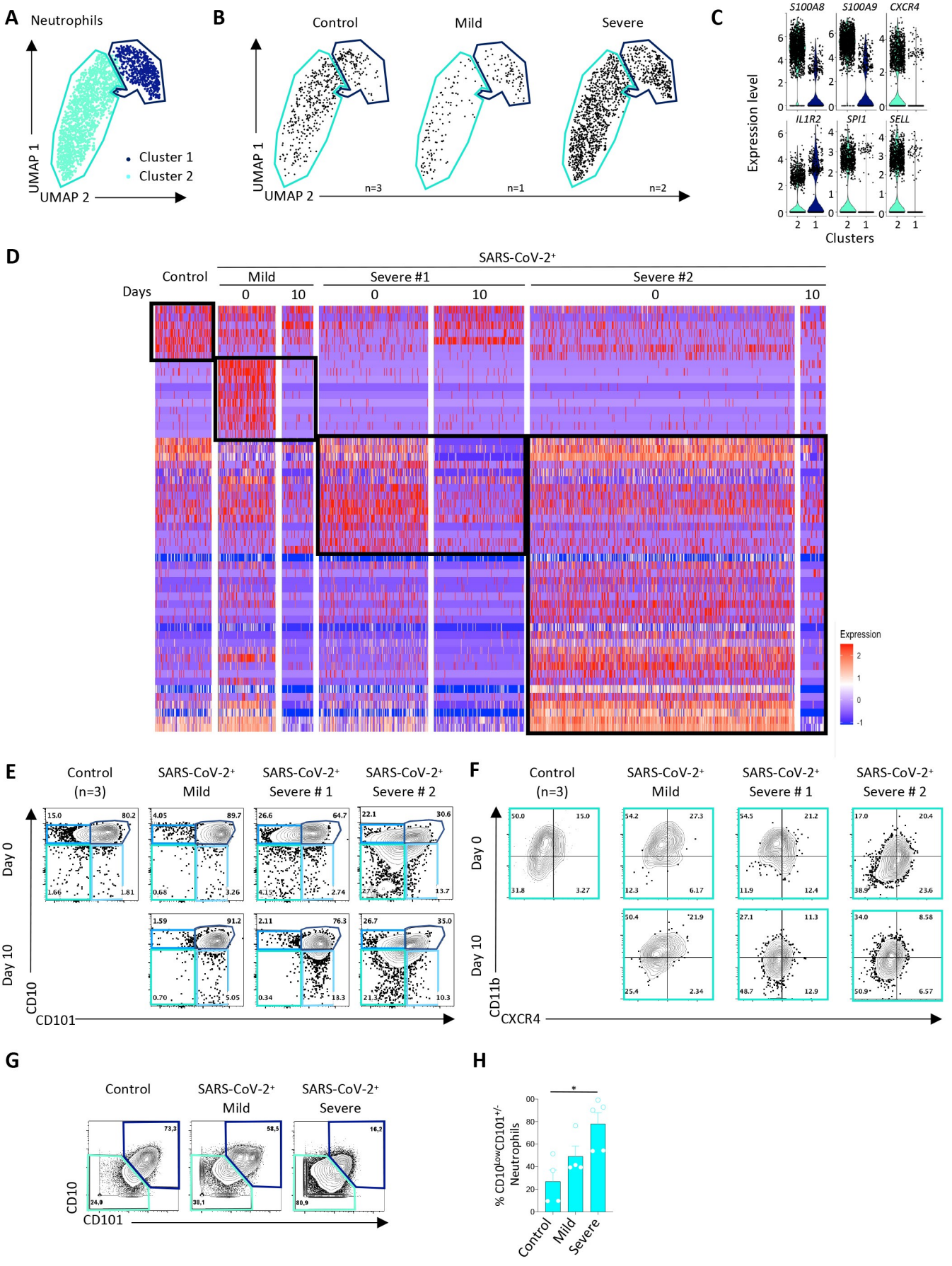

Silvin A et al, Figure 5

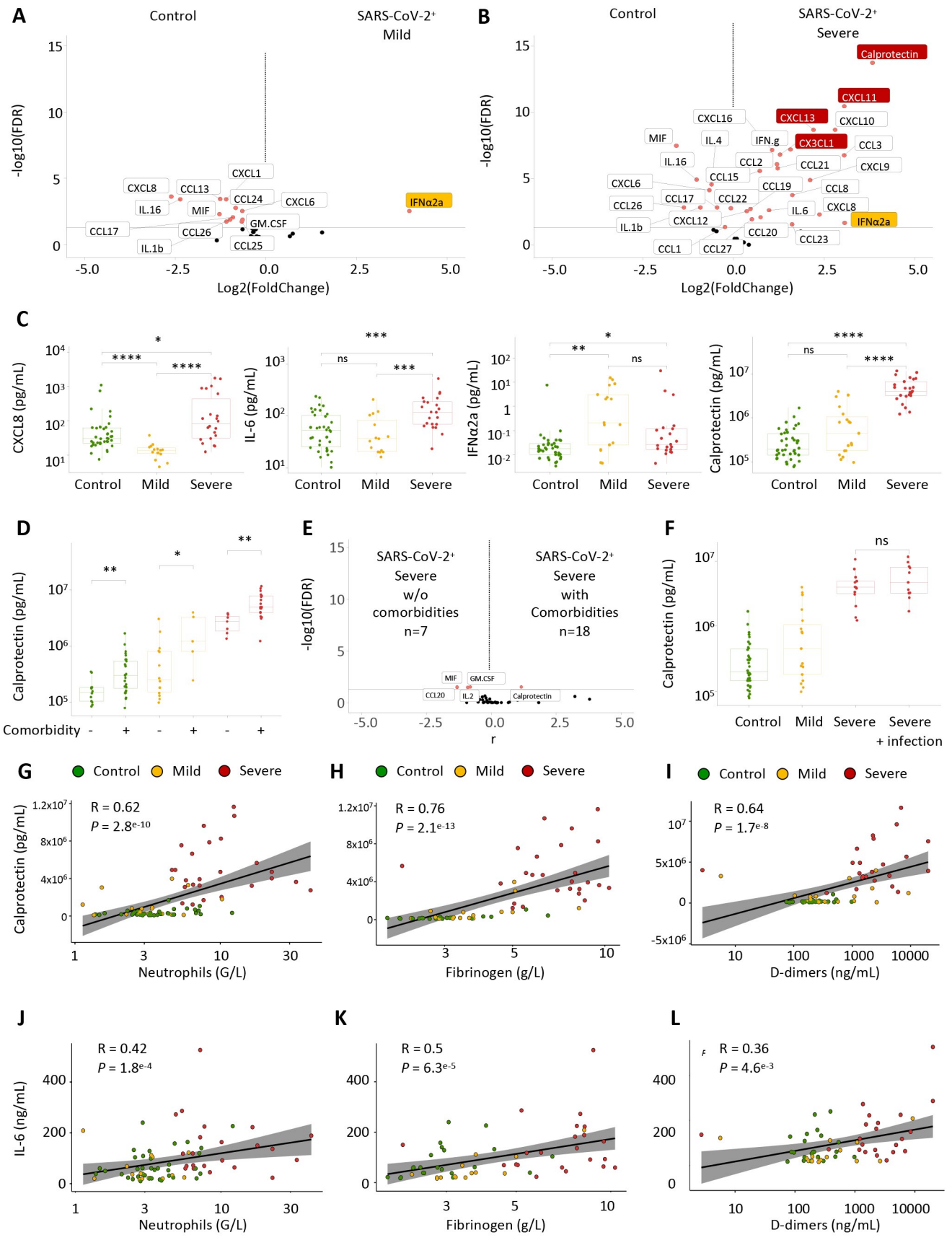

Silvin A et al, Figure 6

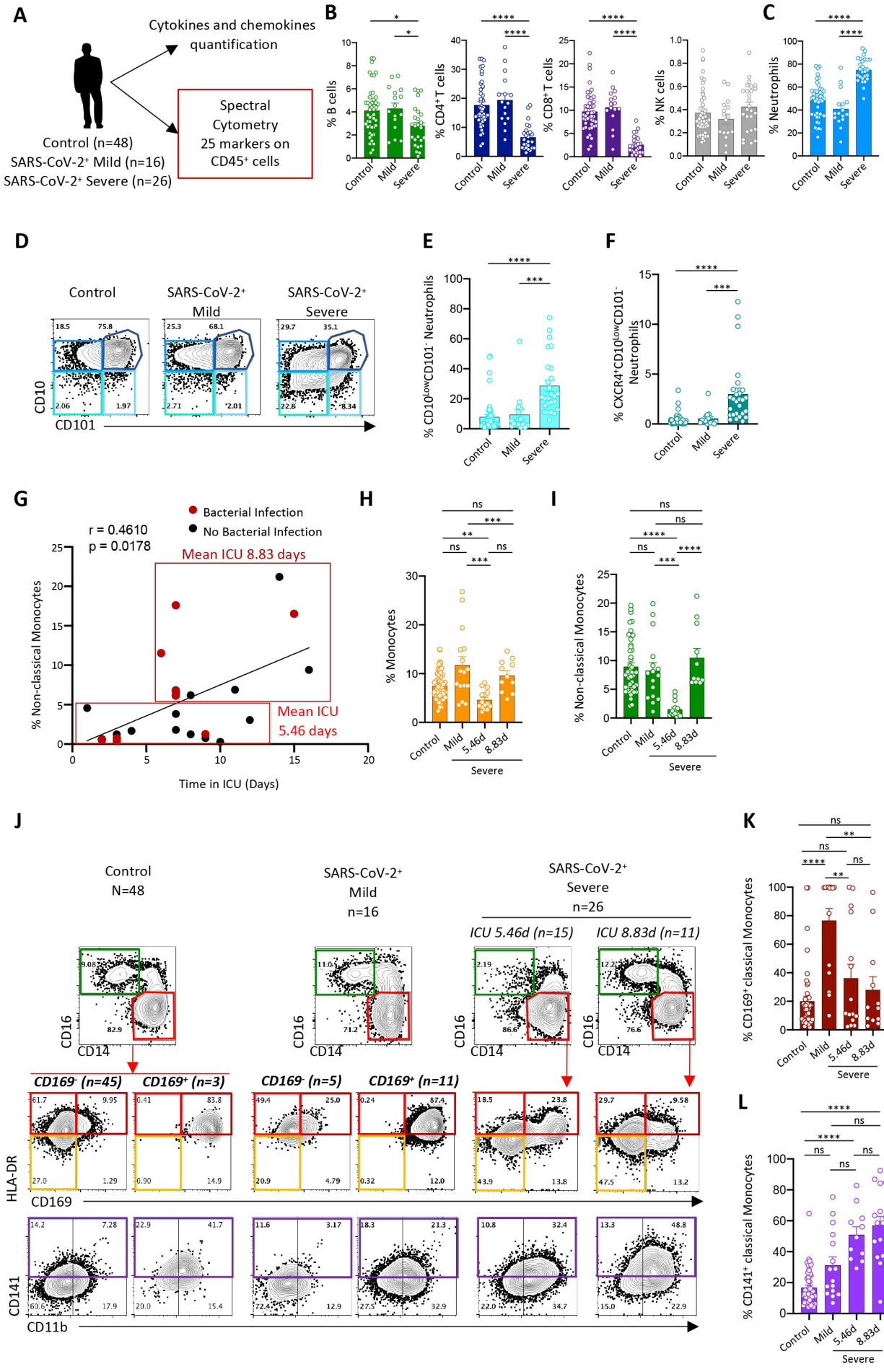

Silvin et al, Figure 7

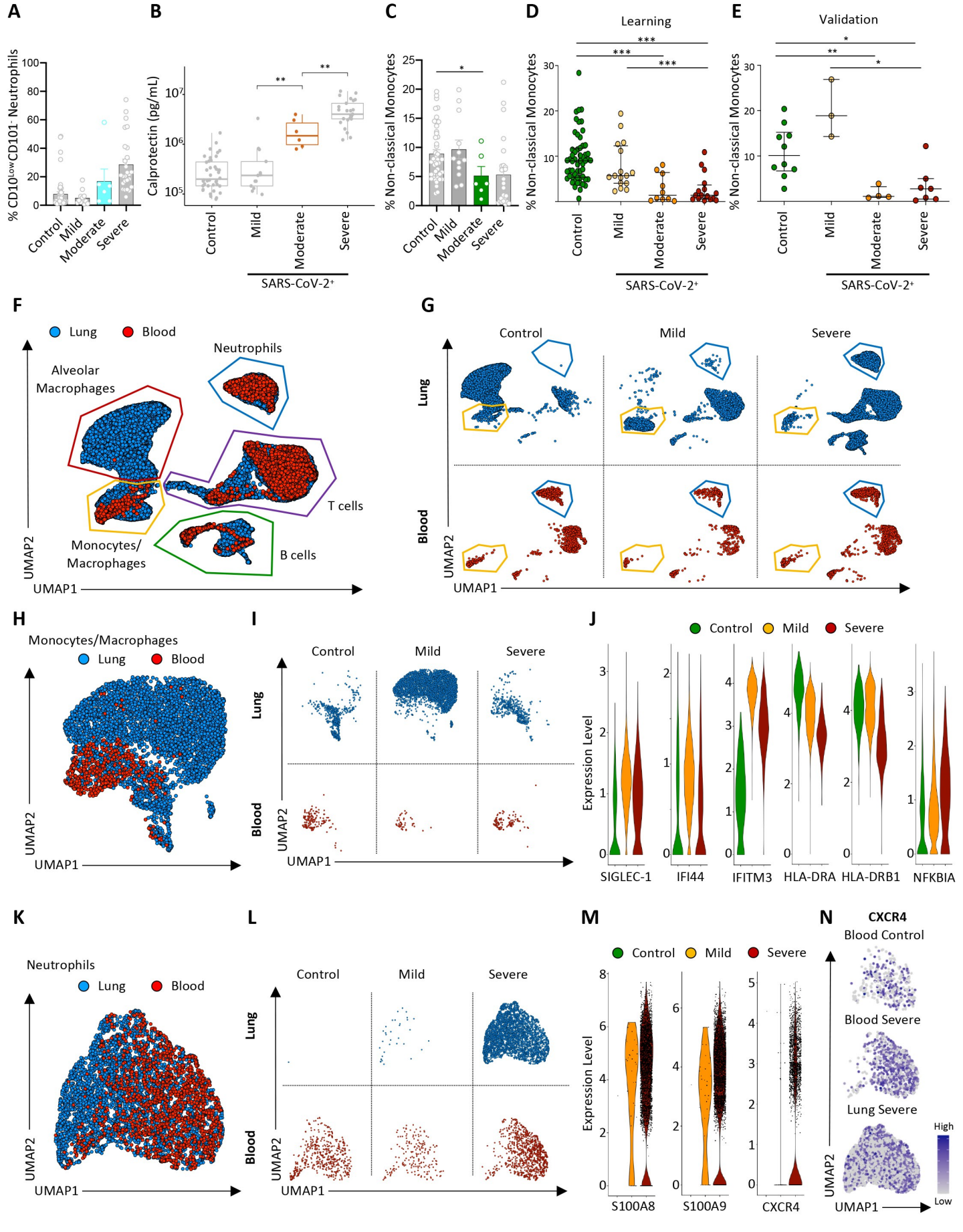

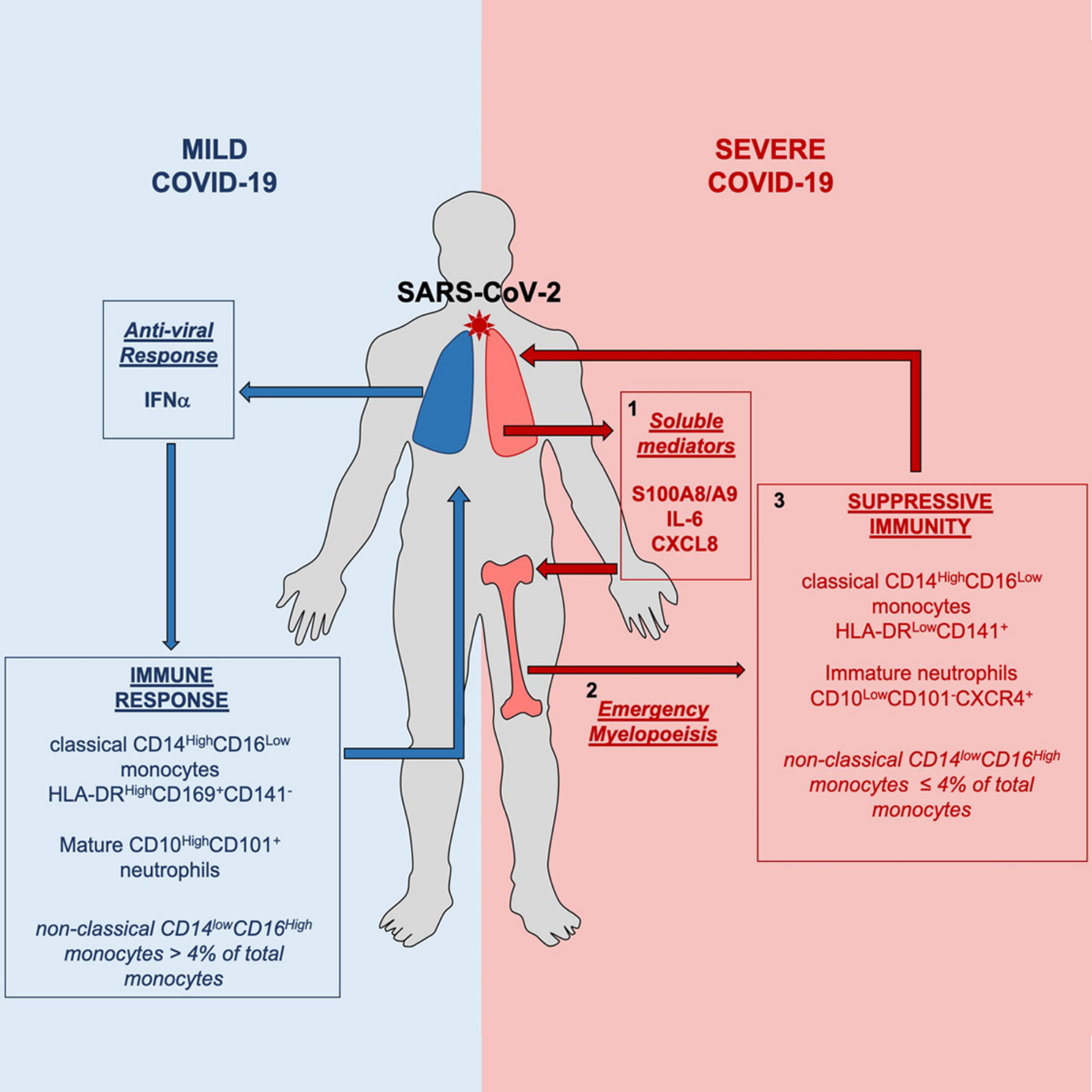
MILD
COVID-19
SEVERE
COVID-19
SARS-CoV-2
Anti-viral Response
IFNα
1
Soluble mediators
S100A8/A9
IL-6
CXCL8
3
SUPPRESSIVE IMMUNITY
classical CD14HighCD16Low monocytes
HLA-DRLowCD141+
Immature neutrophils
CD10LowCD101-CXCR4+
non-classical CD14lowCD16High monocytes ≤ 4% of total monocytes
2
Emergency Myelopoeisis
IMMUNE RESPONSE
classical CD14HighCD16Low monocytes
HLA-DRHighCD169+CD141-
Mature CD10HighCD101+ neutrophils
non-classical CD14lowCD16High monocytes > 4% of total monocytes